DYNAMIC MODELING AND PERFORMANCE ANALYSIS OF AN AUTONOMOUS AND NON-AUTONOMOUS MICROGRID

By

Bishop Poudel
22171003

A project submitted to the Department of Electrical and Electronic Engineering in partial fulfillment of the requirements for the degree of
Master of Engineering in Electrical and Electronic Engineering

Department of Electrical and Electronic Engineering
Brac University
August 2022

Declaration

It is hereby declared that

1. The project submitted is my own original work while completing degree at Brac University.
2. The project does not contain material previously published or written by a third party, except where this is appropriately cited through full and accurate referencing.
3. The project does not contain material which has been accepted, or submitted, for any other degree or diploma at a university or other institution.
4. I have acknowledged all main sources of help.
5. I would like to request the embargo of my project for 12M from the submission date due to the plan of publishing it as a research paper at the conference.

Student's Full Name & Signature:

Bishop Poudel
22171003

Approval

The project titled “Dynamic Modeling and Performance Analysis of an Autonomous and Non-autonomous Microgrid” submitted by Bishop Poudel has been accepted as satisfactory in partial fulfillment of the requirement for the degree of Master of Engineering in Electrical and Electronic Engineering.

Examining Committee:

Supervisor:
(Member)

_____

Dr. Abu Hamed M. Abdur Rahim
Professor, Department of Electrical and Electronic Engineering
Brac University

Internal Examiner:
(Member)

_____

Dr. A.S. Nazmul Huda
Assistant Professor, Department of Electrical and Electronic Engineering
Brac University

Department Chairperson:
(Chair)

_____

Dr. Md. Mosaddequr Rahman
Chairman and Professor, Department of Electrical and Electronic Engineering
Brac University

Ethics Statement

This is to certify that this project entitled “DYNAMIC MODELING AND PERFORMANCE ANALYSIS OF AN AUTONOMOUS AND NON-AUTONOMOUS MICROGRID” is the result of my study for partial fulfillment of the requirements for the degree of Master of Engineering in Electrical and Electronic Engineering under supervision of Dr. Abu Hamed M. Abdur Rahim, Professor, Department of Electrical and Electronic Engineering, Brac University and the same work has not been submitted or published elsewhere for the award of any other degree. The research papers, journals, articles, etc. which were referred to during the project are properly acknowledged here in the reference section.

Abstract

A microgrid system with a power system grid connection is advantageous because it can depend on the power grid when additional power is needed. Alternatively, it can also feed the grid with its excess generation. This project looks into the dynamic behavior of a microgrid when it switches from non-autonomous to autonomous mode. Non-linear dynamic model of non-autonomous as well as autonomous systems for a PV-wind-microalternator-STATCOM integrated microgrid system has been developed. Non-linear state equations for the various components of microgrid are modeled in terms of a 28^{th} order dynamic model. The performance of the system is also evaluated by solving the differential equations through MATLAB ode programs. The power generated by three different generating sources are fed to the point of common coupling (PCC) so that the excess generation can be supplied to the main grid. The effect of temporary and permanent fault in the system network has been investigated. A STATCOM controller connected to the microgrid gives voltage support to the system during contingencies. Simulation results suggest that the proposed model can effectively operate in non-autonomous mode until severe disturbance is encountered in the main grid. It also shows that it is capable of switching to the autonomous mode once the disturbance is found to be severe or if it persists for a longer time. The results also shows that the fluctuation in the output waveform is minimum during the period of transition.

Keywords: Microgrid, STATCOM, autonomous microgrid, non-autonomous microgrid, storage device.

Dedication

DEDICATED

TO MY

BELOVED PARENTS

BROTHER

FRIENDS

&

SUPERVISOR

Acknowledgement

This endeavor would not have been possible without the regular guidance, continuous support, and invaluable suggestions from my project supervisor, Prof. Dr. Abu Hamed M. Abdur Rahim. The door to Prof. Rahim's office was always open to me whenever I encountered trouble or had queries related to the project. I will always be indebted to him.

Also, I would like to extend my warm and heartfelt gratitude to my Department Graduate Coordinator, Prof. Dr. Shahidul Islam Khan, for his encouragement and tutelage throughout the duration of the project.

I would also like to give special thanks to the University as a whole and also specifically to the International and Scholarship Office for their cooperation and assistance by providing me with financial support and resources needed for the successful accomplishment of the project.

Last but not the least, my deepest thanks to my beloved parents, brother and friends for their immense love, endless support and inspiration since the start of the project, which kept me feeling motivated, energized and confident to bring the project to its final stage.

Table of Contents

List of Figures

List of Acronyms

AC	Alternating Current
BESS	Battery Energy Storage System
BPSX	BP Solar Corporation’s
CCM	Continuous Conduction Mode
DC	Direct Current
DCM	Discontinuous Conduction Mode
DERs	Distributed Energy Resources
DFIG	Doubly-fed Induction Generator
DG	Distributed Generation
ELC	Electronic Load Controller
FACTS	Flexible Alternating Current Transmission System
GC	Grid-Connected
GS	Grid Side
GSC	Grid Side Controller
IGBT	Insulated-Gate Bipolar Transistor
IS	Islanded/Isolated
KCL	Kirchhoff’s Current Law
KVL	Kirchhoff’s Voltage Law

LVRT	Low Voltage Ride Through
MPPT	Maximum Power Point Tracking
MS	Machine Side
MSC	Machine Side Controller
MW	Mega Watt
NREL	National Renewable Energy Laboratory
PCC	Point of Common Coupling
PCU	Power Conditioning Unit
PMSG	Permanent Magnet Synchronous Generator
PQ	Power Quality
PV	Photovoltaic
PWM	Pulse Width Modulation
RES	Renewable Energy System
SMES	Superconducting Magnetic Energy Storage
STATCOM	Static Synchronous Compensator
VAR	Volt-ampere Reactive
VSC	Voltage Source Converter
WECS	Wind Energy Conversion System

Chapter 1

Introduction

1.1 Background and Motivation: Distributed Generation and Microgrid

The increasing energy crisis, environmental issues, and ecological disruptions are signs of more power demand and an increment in global warming in the near future. Many organizations are collaborating with local and governmental bodies to reduce these environmental-related issues and to increase the generation of green and clean power.

Since 1950, the amount of carbon dioxide in the atmosphere has increased by 30%. Coal, natural gas, and oil are the three most frequent types of fossil fuels that were being used with coal accounting for 45%, natural gas for 20%, and oil for 35% of carbon dioxide emissions in 2015 [1]. These days, the interest in utilizing renewable energy sources for minimizing the energy crisis and global warming has been increasing. Various types of distributed generation (DG) units with different power conversion and power transfer techniques are being implemented for generating power on a small or medium scale. The small-scale generators are linked to facilitate power transfer to the main grid and to supply local load connected to the microgrid during normal/abnormal conditions in the system network.

DGs are divided into two different types: inertial and non-inertial. DGs such as internal combustion engines, and gas turbines fall under inertial DGs; while DGs such as wind systems, photovoltaic (PV) systems fall under the non-inertial category. Inertial machines are rotating in nature and can provide physical inertia, low sensitivity to parameter variations, and switching harmonics during disturbances. This helps in retaining the system back to a steady-state when temporary disturbances or faults are encountered in the power system network. On the contrary, non-inertial systems require various power electronic devices such as converters,

capacitors, and inverters for converting obtained power into AC at a desired voltage level and frequency. Due to a lack of physical inertia, this type of DG system has limited load capacity and is much more sensitive to parameter variations and switching harmonics [2].

Besides DG systems, there are microgrids which are long been used to power off-grid villages, military operations, and industrial enterprises in remote places; and are defined as a cluster of loads and distributed generators operating under a unified controller within a certain local area either in a grid-connected (GC) or isolated/islanded (IS) mode. These days, they are rapidly being employed in cities, urban centres, universities, hospitals, and data centres. It is directly or indirectly assisting communities to become more energy independent and to reduce environmental pollution. It also helps to improve grid resiliency and to alleviate grid disturbances by serving as a grid resource for quick system response and recovery. Because of various advantages and due to the abundance of high-potential renewable energy supplies, the focus of current power system experts have been shifted from centralized power generation to microgrid systems.

Around 800 million people do not have access to electricity, and 2.7 billion have only limited access. The cost of establishing microgrids is a major concern, as the World Bank estimates that 200,000 microgrids would be required in emerging nations by 2030. According to a survey by the National Renewable Energy Laboratory (NREL) in 2018, microgrids for commercial and industrial consumers in the United States cost around $4 million per MW, with campus/institution microgrids costing $3.3 million per MW, utility microgrids costing $2.5 million per MW, and community microgrids costing $2.1 million per MW [3]. However, with the advent of new technologies, the cost of power converters and inverters has been decreasing, leading to the overall decrement in the generation cost of electricity from DGs.

As a microgrid is specially designed to improve grid resiliency and to power local loads, the modeling and controlling of a microgrid is a significant part of proper power management. The well-modeled microgrid system properly regulates the active and reactive power flow in the network. This activity is essentially carried out by STATCOM (Static Synchronous Compensator) with energy storage devices. At a higher system voltage, the STATCOM absorbs reactive power behaving as an inductor; but at a lower system voltage, it generates and injects reactive power into the system behaving as a capacitor [4]. Thus, the voltage and frequency of the entire system can be improved by altering the STATCOM's active and reactive power flow.

The DG sources that need the use of power electronic converters encounter various operational and stability related issues in a microgrid. As the microgrid contains synchronous sources, maintaining rotor angle and voltage stability is very important. During both normal and emergency settings, the voltage at the point of common coupling (PCC) must be kept within permissible ranges. Large amounts of renewable energy in the system network may have an impact on the voltage at the PCC and also on the rotor angle stability. Other issues that develop as a result of renewable energy integration include the generation of switching harmonics, voltage and frequency fluctuations etc. To reduce these instability issues, microgrid needs control techniques for controlling the power supply. So, all these factors need to be considered for dynamic modelling and controlling of the microgrid system.

1.2 Types of Microgrids

The microgrid can operate in two different modes: non-autonomous (grid-connected) and autonomous (islanded/isolated) modes. The main grid maintains the voltage and frequency of the microgrid, supplies deficit energy, and extracts excess energy in non-autonomous mode; however, in an autonomous mode, the overall renewable energy system (RES) and/or energy

storage system itself supplies the necessary deficit energy to maintain the power supply balance [5].

The ability to shift from non-autonomous to autonomous mode, either intentionally (due to switching for maintenance or any other purposes) or unintentionally (due to sudden fault or disturbances) is the main idea of the microgrid. It has the capability of both generating enough power to deliver to the local load and dumping the excess power using an electronic load controller (ELC) after the transition to the autonomous mode from non-autonomous mode [6].

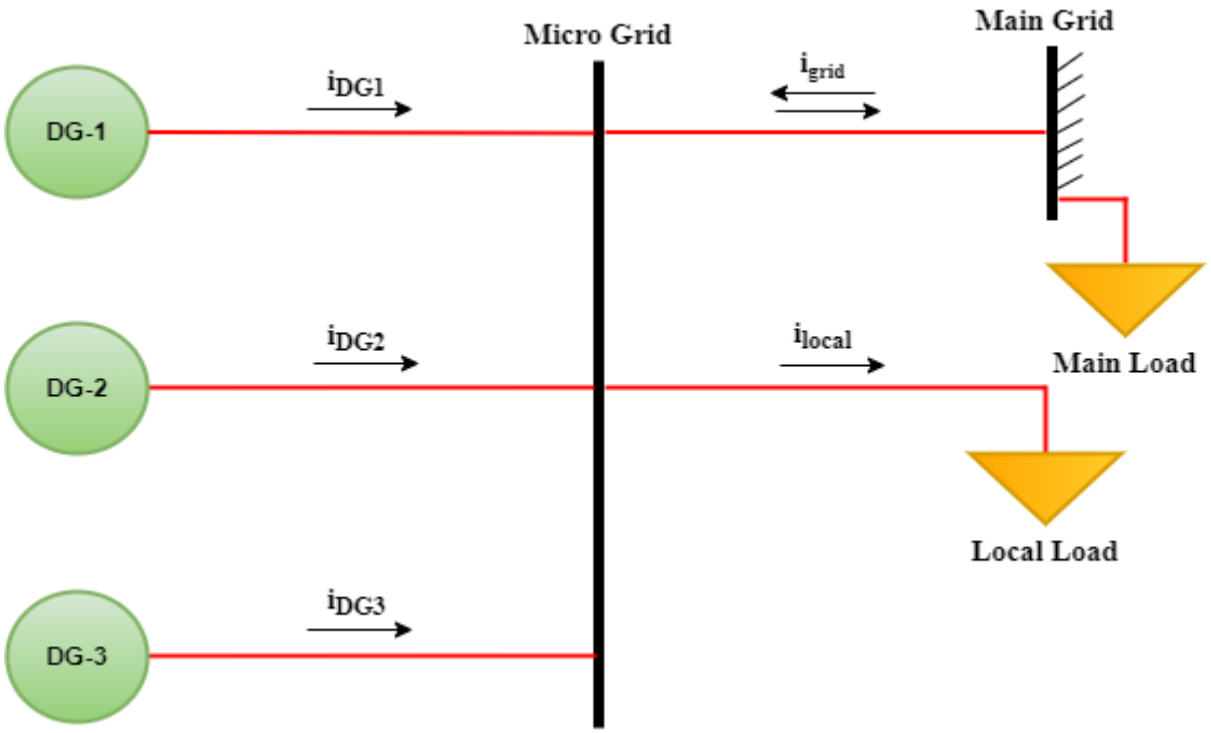

Fig. 1. 1 Non-autonomous mode of operation in microgrid

In the non-autonomous mode of operation of a microgrid, one or more DGs as shown in fig. 1.1 are connected either directly in case of inertial machines or indirectly through power electronic converters and inverters in case of non-inertial machines; and then are fed together to the common grid, commonly known as microgrid or point of common coupling (PCC). In this case, the PCC is connected to the utility grid via a transmission/distribution line. Here, the system voltage and frequency at PCC and grid need to be matched before making the

connection for reliable operation of power flow. The local loads and main loads are connected to the PCC and main grid respectively as shown in fig. 1.1.

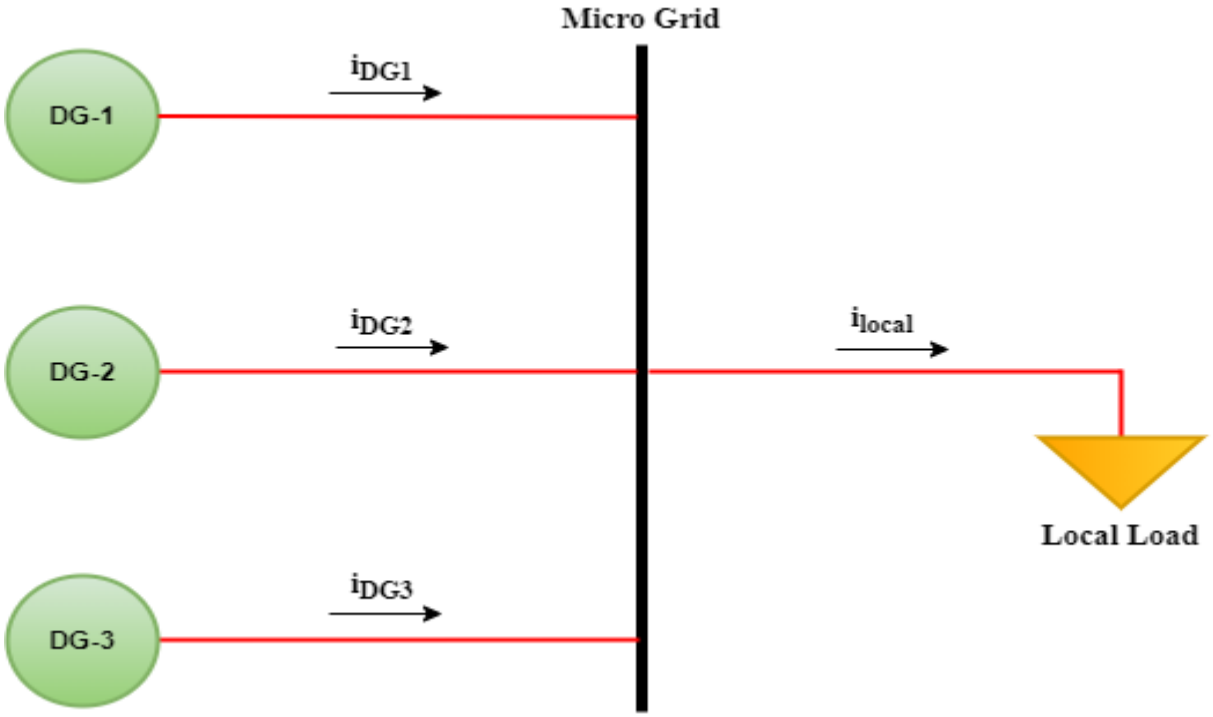

Fig. 1. 2 Autonomous mode of operation in microgrid

In the autonomous mode of operation, one or more DGs as shown in fig. 1.2 are connected together to the PCC in a similar way as in the case of non-autonomous mode. The one difference here is that the PCC is not connected to the utility grid, and the power generated is solely fed to the local loads connected to it. The generation of power also changes according to the demand of the load.

1.3 Control of Microgrid

Though microgrid design seems to be easier and less time-consuming, its overall control is more challenging than it is expected to be. It is necessary to develop some microgrid control techniques for ensuring a smooth transition between autonomous and non-autonomous modes of operation. During the transition process, the control technique used should be able to reduce the voltage/current variations caused by frequency/phase misalignment [7].

Microgrid characteristics alter with generation and system loading, resulting in varied system behavior under different operating conditions. Due to the complex change in the controller parameters, the controller settings that stabilize the system under normal operating conditions may not give adequate results when there is a significant change in the power system operation parameters. Finely tuned controller parameters are needed for ensuring the desired control performance and power quality at varying operating conditions.

The control of microgrid includes both mechanical and electrical controls [8]. Mechanical controls include the control related to the adjustment of input torque pulse. For example, in micro-hydro, it is adjusted by regulating the water flow to the turbine. Similarly in WECS, it is adjusted by controlling the pitch angle and tip speed ratio of the blade. But as there is no rotating parts in PV system, no mechanical control is needed.

As the disturbances and faults in the microgrid system need to be cleared within a few seconds, mechanical-based controlling is not efficient for responding to emergencies. Hence, electrical controls are needed for it to restore the system to a steady state. Different excitation systems, VAR compensators, and energy storage devices are employed for ensuring the proper functionality of the system network during contingencies.

The power flow in a microgrid is controlled using a variety of control techniques. Maximum power point tracking (MPPT) is one of the techniques for extracting the maximum possible power from renewable energy sources. MPPT is performed by ensuring the proper positioning of the main component of the generating sources. For instance, the best positioning of turbine blades in WECS and PV modules in PV systems generates maximum power based on their capability/rating. Also, STATCOM is used for regulating the reactive power for grid resiliency; which thus also helps in regulating the overall power generation. The voltage of the entire system can be improved by controlling the STATCOM's reactive power flow [9].

During a grid fault, the microgrid must withstand voltage dips if within a certain percentage of nominal voltage for a specified period for fulfilling the LVRT criterion. After encountering such voltage dips, it then need to provide quick active and reactive power restoration to pre-fault values. During fault, reactive power support plays much more importance than active power support. Depending on the level of a voltage dip, a reactive current is to be injected into the grid to avoid excess current in the inverter and to regulate the smooth power flow during that time.

The power output of DGs need to be controlled. They are usually set to their rated power, and their steady state frequency is locked to the grid frequency for reliable operation. As a result, an individual DG's active and reactive power requirements need to be determined depending on their rating. Normally, power and voltage references are used to determine the output current reference. The reference value must be re-initialized when shifted from non-autonomous mode to autonomous mode and vice-versa; which then ensures the quick shifting of the system to new steady-state values [11].

The required number and size of compensators need to be used to neutralize the effects of harmonic components produced by local loads while supplying a predetermined amount of active and reactive power. The DG's current and voltage will then get balanced [11]. To reduce the harmonic distortion induced by the inverter switching process from DC to AC, LCL filters are need to be used. The voltage ripple produced by pulse width modulation (PWM) switching is then reduced by this LCL filter [12].

1.4 Statement of Problem

Voltage and frequency management, demand and supply balance of power, power quality, and communication among various components of microgrids are all difficulties that may arise when a microgrid operates in an autonomous mode; while energy security and power flow

management are some major difficulties that a microgrid in non-autonomous mode may face. With all these issues, voltage and current harmonics, voltage sags/swells, voltage and current unbalance, and circulation of neutral currents are some common issues that can occur in both the operating modes [13].

Because of backward power flows from DG units, oscillations in local loads, transient modes in microgrid, demand-supply uncertainties in the network, significant frequency deviations in an autonomous mode, these days the microgrid's main concerns are in stability, protection, and reliability [14].

Due to the high penetration of distributed energy resources (DERs), a reduction in synchronous inertia is prominent as most of DERs are non-inertial in nature. In other words, when compared to systems with solely conventional synchronous generators, the microgrid's resilience to any kind of disturbance is weakened, resulting in a higher rate of change in frequency. In the case of a sudden mismatch in the injected and/or absorbed power, a significant deviation in frequency occurs in the microgrid [15]. This could also influence both rotor angle and frequency stability; while a reduction in short-circuit strength and reactive power reserve could create voltage and rotor angle stability problems in the power system network [16].

Due to the irregularity of generation from DERs, the transition from a synchronous generator-based conventional power generation to converter-based RESs degrades the frequency stability of the power system [17]. The lack of rotational inertia, in contrast to conventional power generation, thus becomes the principal issue in connecting RESs to the electrical grid via power electronic converters.

Among many problems, the dc-link voltage regulations of RESs to some constant is one of the challenging problems in a microgrid. If no action has been performed in the regulation of the

dc-dc converter during a voltage sag, the power from the DGs is not reduced, and the dc-link voltage keeps on rising continuously exceeding the higher permissible limit [18].

In a non-autonomous mode of operation, the droop control relations P-f and Q-V operate effectively only when the X/R ratio of the distribution lines is significantly higher than unity. When the microgrid shifts from non-autonomous mode to autonomous mode, the X/R ratio of linked lines approaches to unity or less than it. This has a major impact on droop power-sharing relationships and increases the active and reactive power coupling, lowering controller performances [19].

On smooth transitioning of a microgrid from non-autonomous mode to autonomous mode and vice-versa, fluctuation in frequency may occur and may also distort the power angle [19]. Also, due to the switching operation in operating modes, the deviation in inverter outputs may be large leading to a complete shut-down of power flow to the consumer end.

Among all these issues, the major problems which motivated to start this project are the switching harmonics and flickers seen in the output waveform during the transition from non-autonomous mode to autonomous mode.

1.5 Objectives of the Project

This project primarily focuses on mathematical modeling and effective ensurance of performance of a microgrid with both conventional power generation based (microalternator) and power-converter based DERs (PV and wind) in integration with STATCOM. The system is aimed to be designed in such a way that it can effectively work in both autonomous and non-autonomous modes.

Some additional aims and objectives of this project are listed below:

- To reduce voltage-frequency fluctuations at the PCC and main grid.

- To use the STATCOM for reactive power support in both autonomous and non-autonomous modes.
- To analyze the steady state and transient performance of the microgrid through the MATLAB ode program.
- To ensure the dc-link voltage of the power-converter to remain constant or within a certain specific range throughout the operation of the microgrid during normal/abnormal conditions.
- To ensure effective transition from non-autonomous mode to autonomous mode during severe fault in the main grid.
- To see the individual and overall performance of the system model under the condition of faults/disturbances in both autonomous and non-autonomous modes.

1.6 Project Outline

The project report is organized as follows:

Chapter 1 introduces the overall work done in this project. The background details of microgrids and DGs are presented with their different types and control mechanisms used. The common issues related to the microgrids are figured out, and various aims and objectives set for its solutions are also included here in this chapter.

Chapter 2 includes the literature review performed throughout the project. The research papers, journals, and articles that were referred for the detailed study of various components of microgrid, its stability related issues; and the suitable control measures currently being used are included in this section.

Chapter 3 presents the non-linear models of various components of PV-wind-microalternator-STATCOM integrated microgrid. The state variables and thus state equations are determined for using it in the MATLAB ode program.

Chapter 4 illustrates the overall system model taken into consideration for the project. The non-linear system operating in an autonomous and non-autonomous modes is presented here. Necessary calculations performed are also included in this chapter.

Chapter 5 presents the various system responses obtained by simulating the non-linear state equations of the microgrid models. The analysis made on the obtained plots is also included here in this chapter.

Chapter 6 illustrates the main findings and conclusion of the project. It also includes the future work that can be done in this area.

Chapter 2

Literature Review

In this chapter, the literature survey done for the successful accomplishment of the project is summarized. This chapter is categorized into four major sections. The first section compiles the related studies done on different components of a microgrid system taken into consideration; i.e. photovoltaic (PV) system, wind energy conversion system (WECS), microalternator system, and static synchronous compensator (STATCOM). The second section is related to the study of the integrated microgrid and its operation in autonomous and non-autonomous modes. In the third section, the stability issues mainly seen in the microgrid system are focused on. Finally, in the fourth or the last section, the various controlling measures that can be implemented for the proper operation of the microgrid are summarized.

2.1 Components used in Microgrid Model

Various generating sources, power converters, filters, etc. are needed for forming the microgrid. All these components are necessarily used in both the autonomous and non-autonomous modes of microgrid operation. The major component here in the microgrid is distributed energy resources (DERs) for power generation. Microgrid basically consists of two major types of DERs, namely inertial or rotating type DERs, and non-inertial or stationary or inverter type DERs. Rotating type DERs do not require power-converters as they can directly generate and connect AC power to the grid; but stationary type DERs need power-converters for proper coupling to the grid [20]. Microalternator used in this project falls under rotating nature while PV and WECS fall under inverter type DERs.

Besides DERs, power converters such as AC/DC or DC/AC converters are used as an intermediate component for connecting the power generated by DERs to the grid at the desired

level of voltage and frequency. The harmonics in the output current are then filtered by LC or LCL filter placed in between the inverter and the grid.

2.1.1 Photovoltaic (PV) System

A PV system is formed by the grouping of the number of solar cells. The solar cells are connected in series forming PV modules and these modules are then connected together in a series-parallel arrangement to form a PV array. PV system is defined as any system with a p-n junction that can convert solar energy into electric charge and thus into a usable form of electricity [21, 22]. When the sun rays incident on the solar panel, and when these incident photons pass the threshold to remove the electrons from the valence band breaking its covalent bond, then these charge carriers start to transport at the p-n junction, which then generates electricity [23, 24].

In the literature, different research papers, journals and articles followed show that the mathematical modeling and controlling of PV modules is not an easy task as many parameters are needed to be considered. Besides providing theoretical methods for modeling of PV, some researchers have also offered a practical method for its modeling. However, a strategy needs substantial testing at five different discrete operational points. Because of all these complexities, these types of models are rarely used [25]. So, for ease of work in this project, the model of PV cell obtained from the manufacturer's datasheets has been taken into consideration. The model used here is named BP Solar Corporation's BPSX-150 [26].

A PV model with power-electronic components is also studied in the literature [27, 28]. The thorough model investigates the overall system and its control measures; however, it is complex in real implementation [29, 30]. These models are suitable for steady-state analysis, but cannot be adopted for dynamic studies.

To match the experimental data collected from a specific PV module with a voltage source converter, a PV transient model has been studied [18]. The control action was found by deriving mathematical relations that demonstrate the model equations' independency from the PV system considered. The NREL produced simple model of a PV system in which the PV system was treated as a regulated current source, considering the current and phase angle are also studied [31].

2.1.2 Wind Energy Conversion System (WECS)

In recent years, the use of wind energy for power generation has been increasing rapidly due to its many financial and environmental benefits. WECS incorporates two sequential conversions; i.e. one direct conversion into mechanical power and another indirect conversion into electricity or electrical power by the use of various mechanical and electrical components [32].

In WECS, the kinetic energy from the wind when passes between the turbine blades, it makes turbine blades to rotate with a very high speed. As the shaft of the turbine and generators are coupled together, this rotation of turbine blades makes the rotor of the generator to rotate at the same speed. The energy generated by the generator is then connected to the microgrid or to the main grid by using various power electronic equipments.

There are various types of generators that can be used in WECS. Among all, the most commonly used generators are permanent magnet synchronous generator (PMSG) and doubly-fed induction generator (DFIG) as they are much more efficient for generating huge power even at the variable speed of wind [33]. PMSG is a self-excited ac generator used in WECS. It has its own permanent magnet, which is responsible for generating a magnetic field, and hence they do not need any dc source for excitation [34]. DFIG is also another commonly used generator in WECS. Here in DFIG, the transformer is employed between its stator and grid;

and the harmonic filter is used between the rotor and the grid. To gain variable speed, its rotor is supplied with an external varied voltage via slip rings [35]. The power converters and other power-electronic devices are used in WECS for reducing the overall mechanical stress in the system; which thus helps on making the system more reliable and efficient [36]. The power electronic components plays a significant role in both fixed and variable speed wind turbine systems. The use of these components also assists in eliminating the use of gearbox in the WECS, which can ultimately decrease the losses and damages in the overall system.

In WECS, three different systems are needed to be controlled together for the control of overall system. They are pitch angle control, machine side (MS) control, and grid side (GS) control [37]. In pitch angle control, the turbine blade speed and aerodynamic power generated are controlled by changing the angle of turbine blades. In MS control, the machine side controller (MSC) plays a significant role in extracting the maximum power by the principle of MPPT; i.e. by changing the blade angle to gain maximum power. In GS control, the grid side controller (GSC) does not play any specific role in the conversion of power but it is needed for improving the power quality before synchronizing it to the grid.

2.1.3 Microalternator System

Microalternators are the DERs that are made for consuming low power in a highly efficient way. They are known for their great performance, dependability, and long life [38]. Some commonly used microalternators are diesel generators, gas turbine systems and so on. They are commonly employed in agriculture, and construction sites.

In most of the literature, the microalternator is represented by a fourth-order model consisting of power angle, angular frequency, generator internal voltage, and field excitation voltage along the d-axis [39].

Microalternators are easier to control as regulating fuel such as diesel or gas can regulate the overall generated power. They can also directly be connected to the grid without using any intermediate power-converters so the inter-transmission loss is less in microalternator systems than in other commonly used DERs.

2.1.4 Static Synchronous Compensator (STATCOM)

As most of the industrial loads are inductive in nature, the power factor of the system usually goes below unity. So, to maintain the power factor close to unity, extra reactive power support is needed for the system. The reactive power support to the power system network can be provided through various flexible alternating current transmission system (FACTS) devices. There are two major ways of compensating reactive power; i.e., by the use of traditional reactive power generators or by using static reactive power generators. By using shunt capacitors, synchronous alternators and phase-modulation machines, the traditional reactive power compensation is performed. The major disadvantage of this type of compensation technique is that they are not able to track frequent changes in the reactive power of the load. With this disadvantage, they are also noisy and bulky in nature. Another method of reactive power compensation is by the use of a static VAR compensator. In this method, the compensator have a reactor (or static switch) capable of absorbing and emitting reactive current for power factor improvement, voltage stabilization and frequency suppression. In past, these types of compensation devices were slow operating; but now due to the advent of new technology in power-electronic sectors, they are made fast operating; thus can compensate reactive power within one or two cycle [40].

Among many FACTS devices being used in power plants or substations, STATCOM is the most commonly used FACTS device for reactive power support of the system network. Generally, STATCOM have continuously varied capacitive or inductive impedance. To

determine the direction of flow of reactive power (i.e., whether flowing inside or outside) of the system, the impedance value is calculated by controlling the firing angle. As there is the absence of moving parts in the STATCOM, they fall under the category of static VAR compensator.

Different models of STATCOM are studied and analyzed for proper modeling of PV-wind-microalternator integrated microgrid system taken into consideration. Based on DC voltages [41, 42], STATCOM controller [43], type of converter used [44], and switching devices [45], well-suited STATCOM has been modeled. Besides compensating the reactive power need of the system, STATCOM also assists in maintaining the voltage of the system by reducing the voltage flickers. Thus, STATCOM is one of the core parts of the microgrid for ensuring system stability [40].

2.2 Integral form of Microgrid

One or more than one locally available RESs like PV, wind, microalternator, fuel cells etc. can be integrated together to form a microgrid [46]. The microgrid system could operate in both autonomous and non-autonomous modes depending on the need, amount of power generation and the distance from the nearest utility grid or substation. Though the basis for operating the system in both autonomous and non-autonomous modes are almost similar, the level of difficulty and common issues encountered in these two modes are a bit different.

2.2.1 Operation in Non-autonomous or Grid-connected Mode

In present days, due to the advancement of power converters and switches, the microgrid can be effectively coupled to the utility for supplying power to the main grid or receiving from it. When the demand of local load at the PCC is less than the power generated by DGs, then in such a case, the local frequency increases and the excess power is needed to be supplied to the main grid. In contrast, when the local load demand exceeds the total amount of power

generation by DGs, the local frequency decreases; and the power for the local load need to be received from the main grid [47].

In a non-autonomous microgrid, the synchronous grid-connection strategy is implemented for the control of the switch placed between PCC and the main grid. The control strategy helps on frequency and phase angle detection. Here, separate detection of inverter output voltage and frequency is performed. On comparing these values with the references, frequency and phase deviation are determined and if it meets the grid code, the grid-connection signal as output makes the switch to close [48].

When there is any large disturbances in the utility grid or when the microgrid needs to run independently, the microgrid should be separated from the utility grid and allowed to operate in an autonomous mode as soon as possible [49]. In literature [50], a control strategy for controlling the current harmonics of the inverter is proposed. P-f and Q-V control techniques is also stated in this literature.

2.2.2 Operation in Autonomous or Isolated/Islanded Mode

The grid formed by locally generated renewable power from different power producers has been replacing the conventional centralized grid these days [51]. The grid thus formed is commonly known as an autonomous or isolated or islanded or standalone microgrid. In this type of operating mode, the microgrid itself needs to generate and manage its voltage, frequency and power. So, a well-suited voltage, frequency and power control strategy is needed to be implemented for its proper operation [52].

The autonomous microgrid control techniques are divided into three major steps; namely, primary control, secondary control and tertiary control. The primary control is also called local control as it only focuses on controlling voltage and frequency locally. Still after primary controlling, as there might be a chance of obtaining voltage and frequency deviation, it is then

compensated by the secondary controller. This control ensures desired quality of power and makes energy management of the microgrid. The tertiary control takes place in the case of multiple microgrids and is used between multiple microgrids and the main grid to regulate power quality by managing energy between microgrids and the main grid [53].

2.3 Stability Issues in Microgrids

Different stability related issues can be encountered during the operation of microgrid. The use of electronically connected DG units causes problems like network disruptions, generation of switching harmonics, DG overloading, flickers in distribution transformer, decrease in fault ride through capability and so on. Due to these disturbances, the overall stability and its control are severely harmed. Unlike regular power generating units, the majority of DG units used in microgrids do not contain rotating parts and thus do not respond to frequency change when the load changes. The connecting inverter thus need to be programmed in such a way that it can mimic the inertia of the synchronous generator [54].

The various power quality problems seen in microgrids are frequency and voltage deviation due to reactance, charging and leakage currents, low power factor and so on [55]. For accommodating the components of switching frequency, a well-designed filter can be used; making the impact on the control bandwidth to a minimum. [56] provide a filter with an isolating transformer and a complementing controller to reject various disturbances. The literature [57] presents the harmonic disturbances obtained due to the interactions of a number of inverters in parallel. The solution measures is also proposed here. The voltage fluctuation is settled here by the use of various VAR compensating techniques.

2.4 Control of Microgrids

For the reliable operation of power system network, it needs to be properly controlled. Controlling of microgrid normally deals with reactive power control; as it need to have the

capability of LVRT. The topic of reactive power compensation is generally approached from two perspectives: load compensation and grid-voltage support. The main goal of load compensation is raising the system power factor and balancing the active power drawn by the connected load from various DGs. Similarly, the goal of providing voltage support is to reduce voltage fluctuation at a transmission/distribution line's terminal. By raising the generation of active power by any of the techniques available, reactive power compensation in power systems can be done; which then helps on increasing the system stability [13].

The reliability of supplying continuous power and resiliency to various power quality (PQ) issues are the most desirable aspects of today's power system with DGs. PQ issues coming from the introduction of DGs, as well as due to high penetrating diverse loads are also investigated in literature [58]. The virtual synchronous generator (VSG) systems can be utilized as effective active and reactive power control units to compensate the lack of physical inertia; which thus helps on maintaining the microgrid voltage and frequency [59].

In literature [60], a method of controlling the inverter's operation for the effective integration of DGs into the electrical system is presented. Here, the network's power demand is monitored, and on its basis, the control signal has altered the inverter's voltage angle and magnitude for the desired amount of power transfer.

Chapter 3

Modeling of Microgrid Components

In this chapter, the detailed dynamic model of various DG units and the power-electronic components used to connect to the grid has been presented. The DGs used in this project are photovoltaic (PV), wind energy conversion system (WECS) and microalternator. As non-inertial DGs need a power conditioning unit (PCU), the modeling of interconnecting power-electronic devices like DC/DC boost converter, AC/DC rectifier, DC-link capacitor, DC/AC inverter and the output LCL filter circuit is also performed. For control of microgrid, STATCOM with capacitor energy storage system is also modeled. These developed models are thereafter used as a non-linear system equation in MATLAB ode program.

3.1 Microgrid Configuration

The schematic diagram of the microgrid system considered for this project is shown in fig. 3.1. The system model consists of three DG units for generating electrical power, one STATCOM for central supervisory control, and one lumped (or local) load for consuming generated power. In an autonomous mode of operation, all power produced are consumed by the local loads while in a non-autonomous mode of operation, the generated powers when excess is transmitted to the main/utility grid.

Here, two non-inertial DGs, PV and variable speed PMSG-based WECS are indirectly connected to the microgrid through sequentially placed PCU and filter circuitry; while microalternator system like gas-turbine or a diesel generator is directly connected to the microgrid as it is able to generate power at the required frequency and voltage level. In addition, for supervising and controlling the overall system operation, a STATCOM with a capacitor energy storage device is also interfaced to the system in both an autonomous and non-autonomous modes.

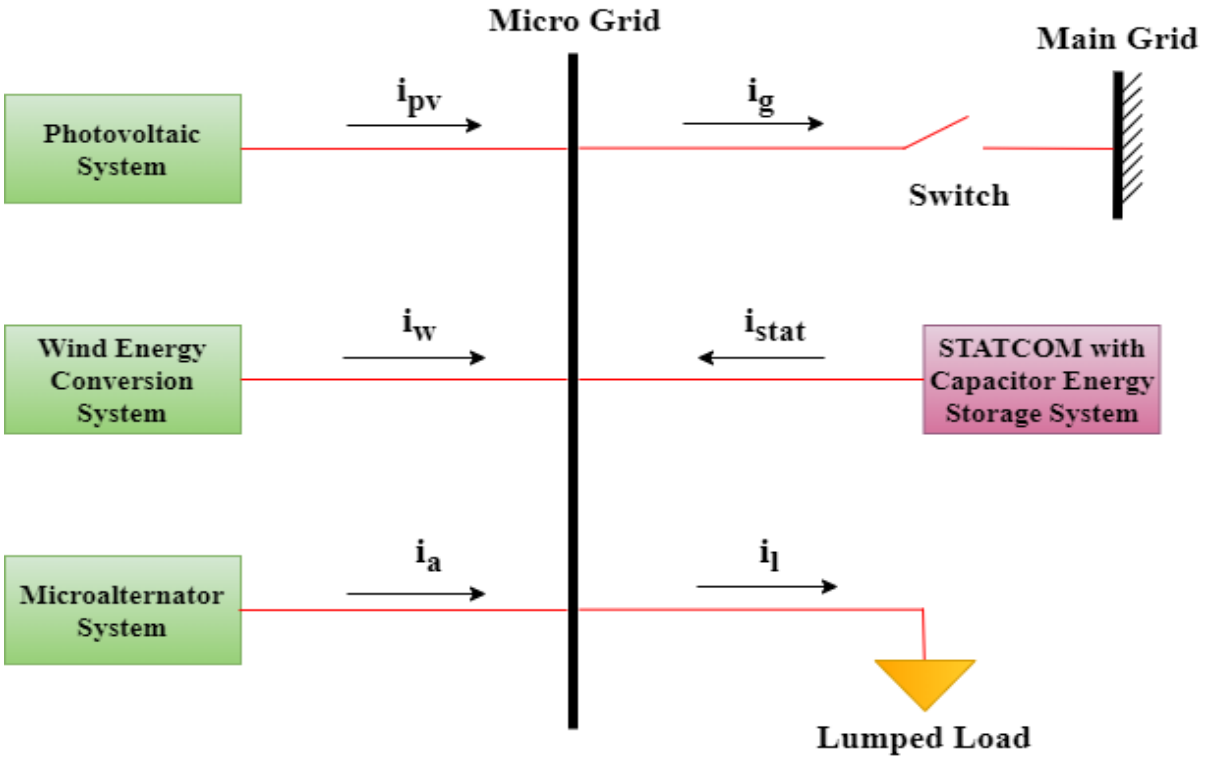

Fig. 3. 1 Microgrid configuration

3.2 Photovoltaic (PV) System

To form a complete PV system, a combination of PV or solar cells made up of n-type or p-type semiconductor is used. Similar solar cells are incorporated together to form PV module; and integration of such modules forms PV panels. The electrical connection of such individual PV panels in series-parallel arrangement ultimately forms the PV system to power the electrical loads.

When sunlight of a suitable wavelength strikes the PV array (particularly, striking on each solar cells), the electrons are ejected and travels to the n-type layer; while the holes formed are collected to the p-type layer. This creates an electric field and when connected to a battery, it stores the electric charge on it; which can later be connected to the microgrid by the use of various PCU and filter circuitry. The working principle of an ideal PV cell and an ideal diode is almost same. The PV output power and current mainly depends on the irradiation level and cell temperature [61]. The effect of irradiation level is proportional to the power output. But

with the increment in cell temperature, the output current is only moderately increased. The increased output current reduces voltage level, which ultimately lowers the output power of the PV system.

For modeling of a PV cell, various components related to it need to be considered. The simple electrical equivalent model of a PV cell consists of a photo current source, a diode, a shunt resistor and a series resistor. The shunt and series resistors are used to represent the leakage current and internal resistance to the flow of electric current respectively [62].

In a PV cell, the incident photon from the sunlight produces a current known as photovoltaic current (i_{ph}). This generated current cannot be fully supplied to the microgrid because of leakage and current flow in the diode.

The net output current of the PV cell (i_{pv}) can be expressed as;

$$i_{pv} = i_{ph} - i_D - i_{sh} \tag{3.1}$$

$$i_{pv} = i_{sc}[1 + \alpha(T - T_r)]\frac{G}{G_o} - i_{rsc}\left(e^{\frac{V_{pv}+i_{pv}R_S}{nV_T}} - 1\right) - \frac{V_{pv}+i_{pv}R_S}{R_{sh}} \tag{3.2}$$

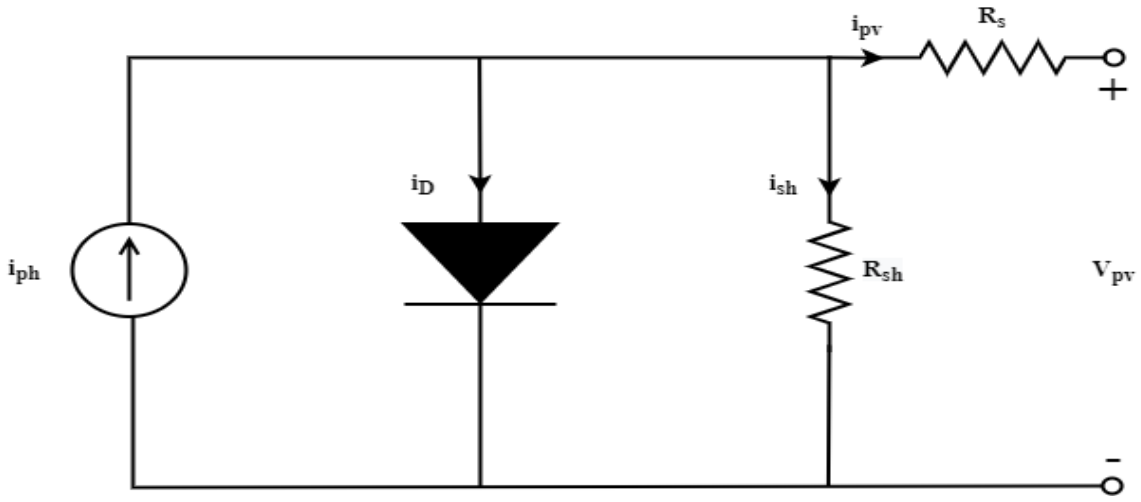

Fig. 3. 2 Simple equivalent electrical model of a PV cell

where, i_{sc} is the PV cell's short-circuit current at 25^0C and 1 kW/m^2, α is the temperature coefficient of i_{sc}, T_r is the reference temperature of the PV cell, G is the irradiation of incident

photon in kW/m^2, G_o is the reference irradiation of incident photon in kW/m^2 i_{rsc} is the reverse saturation current, V_{pv} is the output voltage of the PV cell, n is an ideality factor, R_s is a series resistance, R_{sh} is a shunt resistance, $V_T = \frac{kT}{q}$ is a thermal voltage, $k = 1.380649 \times 10^{-23}\, m^2 kg s^{-2} K^{-1}$ is a Boltzmann constant, T is a cell's operating temperature and $q = 1.6022 \times 10^{-19} C$ is the electronic charge.

Here, the reverse saturation current (i_{rsc}) at any temperature T is given by;

$$i_{rsc} = i_{rscr} \left(\frac{T}{T_r}\right)^{\frac{3}{n}} e^{\frac{-qE_g}{nk}\left(\frac{1}{T}-\frac{1}{T_r}\right)} \tag{3.3}$$

where, i_{rscr} is the reverse saturation current of a PV cell at a reference temperature and solar irradiance, and E_g is the band-gap energy of the semiconductor used in the PV cell.

As the leakage current from the source is inversely proportional to the shunt resistance (R_{sh}) and output power is directly proportional to the series resistance (R_s), the electrical equivalent circuit of a PV cell shown in fig. 3.2 can be reduced to an approximate model by eliminating the shunt resistance. Such a reduced model is presented in fig. 3.3.

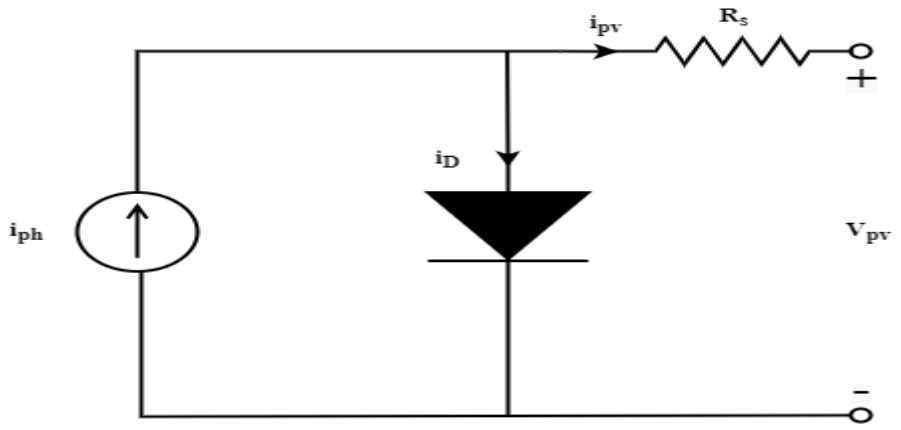

Fig. 3. 3 Approximate model of a PV cell

The net output current for this reduced model is thus obtained as;

$$i_{pv} = i_{ph} - i_D \tag{3.4}$$

$$i_{pv} = i_{ph} - i_{rsc}\left(e^{\frac{V_{pv}+i_{pv}R_S}{nV_T}} - 1\right) \quad (3.5)$$

In practice, the number of PV cells are connected together in series-parallel arrangement for getting a high amount of power from each PV module. In such a case, if the number of series and parallel modules are *Ns* and *Np* respectively, then the equation (3.5) becomes as;

$$i_{pv} = N_p i_{ph} - N_p i_{rsc}\left(e^{\frac{V_{pv}/N_S+i_{pv}R_S/N_p}{nV_T}} - 1\right) \quad (3.6)$$

From (3.6), we observed that the current-voltage relationship of a PV module is non-linear in nature and can be solved by the Newton-Raphson method.

For the PV module, the voltage-current relationship can be expressed as;

$$V_{pv}=N_s\left[ln\left(\frac{N_p i_{ph}-i_{pv}}{N_p i_{rsc}}+1\right)nV_T - \frac{i_{pv}R_s}{N_p}\right] \quad (3.7)$$

Above equation can be written as;

$$f(V) = V - N_s\left[ln\left(\frac{N_p i_{ph}-i_{pv}+N_p i_{rsc}}{N_p i_{rsc}}\right)\times nV_T - \frac{i_{pv}R_s}{N_p}\right] = 0 \quad (3.8)$$

As $f'(V) = 1$, the recursive formula for $(n+1)^{th}$ iteration is;

$$V_{n+1} = N_s\left[ln\left(\frac{N_p i_{ph}-i_{pv}-N_p i_{rsc}}{N_p i_{rsc}}\right)\times nV_T - \frac{i_{pv}R_s}{N_p}\right] \quad (3.9)$$

3.2.1 Power Conditioning Unit (PCU)

As PV system power output is dc, it needs to be converted into the desired ac power level before connecting it to the grid. For this, a PCU is needed to be used between the PV system and the grid. The dominant components used in PCUs are DC/DC boost converter, DC-link capacitor and DC/AC inverter. With this, LCL filter circuitry having coupling inductance is also used at the output terminals of the inverter.

The DC/DC boost converter connected to the output of the PV array boosts the voltage to a certain level. For making this voltage to remain constant throughout the operation, a DC-link capacitor is used in parallel between the boost converter and an inverter. The dc power stored in the DC-link capacitor is then converted to the ac of desired voltage and frequency level by the use of an inverter. But still there might be a chance of getting harmonics and resonance in the power output. In order to reduce it, LCL filter having coupling inductance is incorporated into the system. The complete model of a PV system with various PCUs is presented in fig. 3.4.

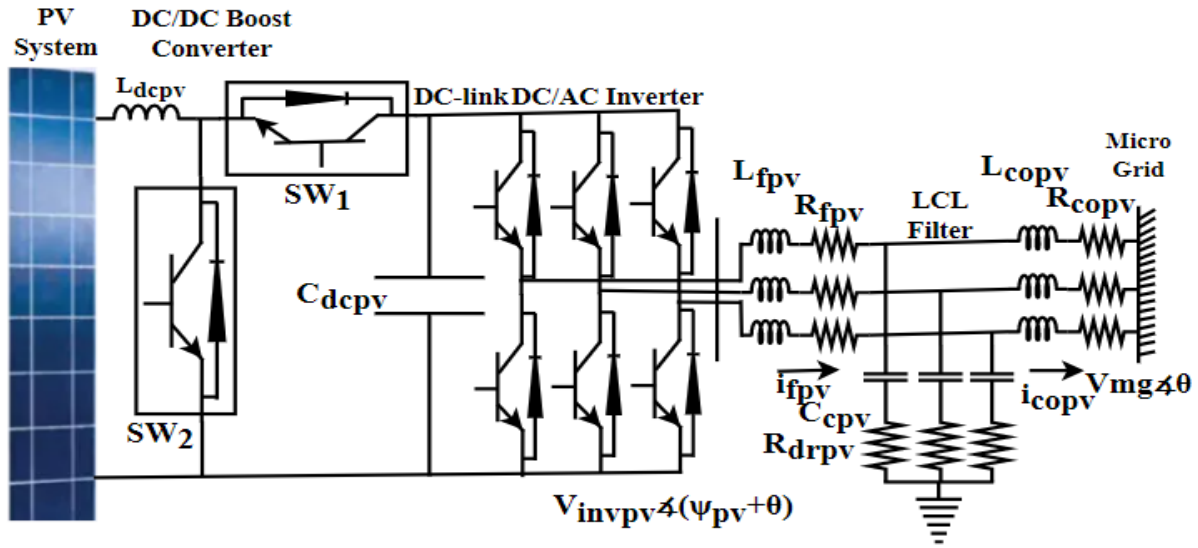

Fig. 3. 4 Interconnection of PCU in a PV system

I. DC/DC Boost Converter

The main function of DC/DC boost converter in a PV system is to increase the output voltage generated by PV with minimum losses during the conversion. It incorporates inductor/capacitor, insulated-gate bipolar transistor (IGBT) switches and a diode to act as a DC/DC boost converter. Here, the inductor/capacitor behaves as a storage element for delivering output voltage with low ripple. This can only be obtained by forming a low bandpass filter [63]. Depending on the duty cycle of the converter, IGBT switches and diode operates to deliver desired dc output voltage.

A DC/DC converter can operate in two modes; namely, continuous conduction mode (CCM) and discontinuous conduction mode (DCM). For continuously supplying power to the grid without any disturbances, here in this project, CCM is implemented. This also ensures that during the fluctuation, the current never reaches to zero.

The basic circuitry of DC/DC boost converter is presented in fig. 3.5. As shown in this circuit, to smoothen the output voltage from the converter, capacitor is used at the output terminal.

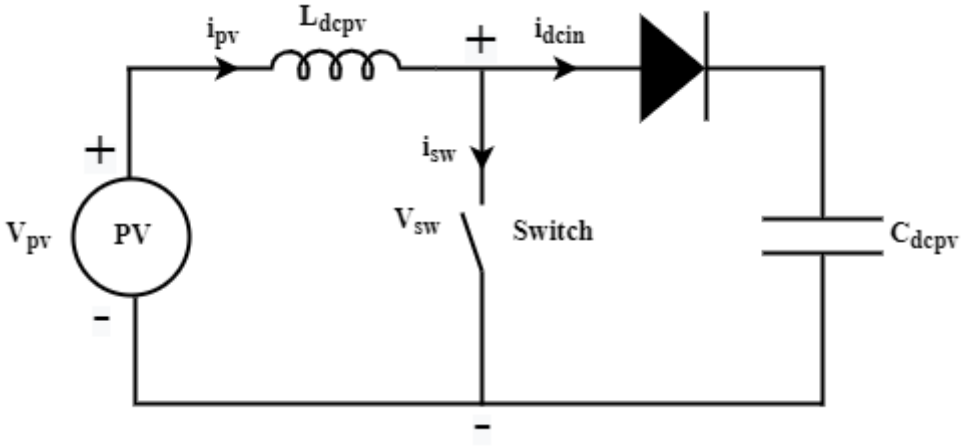

Fig. 3. 5 DC/DC boost converter circuitry model

On considering the output current from PV (i_{pv}) as a state variable; let us apply Kirchhoff's voltage law (KVL) in the first loop of the circuit shown in fig. 3.5. Hence, we get,

$$V_{pv} - L_{dcpv}\frac{di_{pv}}{dt} - V_{sw} = 0 \tag{3.10}$$

where, L_{dcpv} is the inductance of the DC/DC boost converter and V_{sw} is the voltage across the IGBT switch . This V_{sw} can be expressed in terms of duty ratio of converter (d_{pv}) and capacitor output voltage (V_{dcpv}) as;

$$V_{sw} = (1 - d_{pv})V_{dcpv} \tag{3.11}$$

Combining (3.10) and (3.11); the state equation for the DC/DC boost converter becomes as;

$$V_{pv} - L_{dcpv}\frac{di_{pv}}{dt} - (1 - d_{pv})V_{dcpv} = 0$$

i.e. $\frac{di_{pv}}{dt} = \frac{1}{L_{dcpv}}[V_{pv} - (1 - d_{pv})V_{dcpv}] = 0$ (3.12)

II. DC-link Capacitor

The DC-link capacitor by name is an energy storage device linking DC/DC boost converter and DC/AC inverter. It filters out DC output voltage from the rectifier and helps on ensuring constant voltage at the input side of an inverter. Fig. 3.6 shows the DC-link capacitor connected between the DC/DC boost converter and DC/AC inverter.

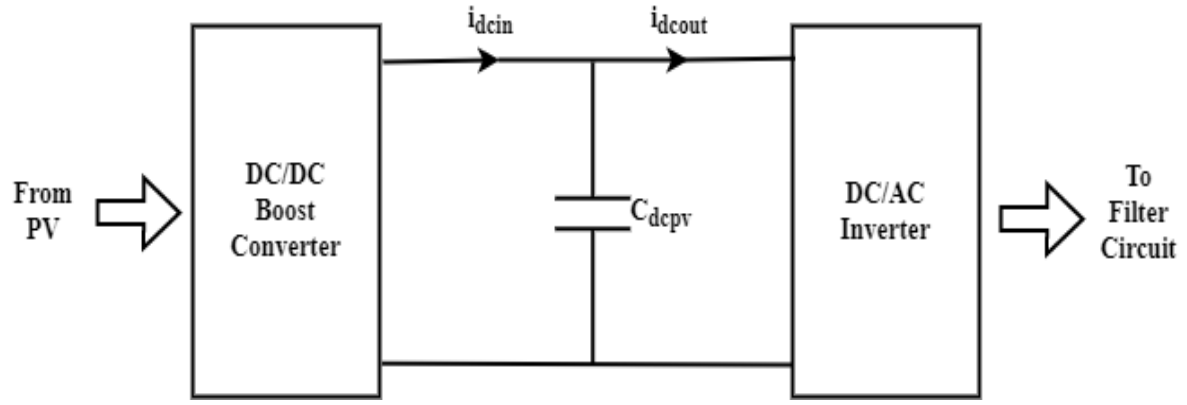

Fig. 3. 6 DC-link capacitor circuitry model

In fig. 3.6, applying Kirchhoff's current law (KCL) at the DC-link junction; we can get the state equation for the DC-link capacitor as;

$i_{dcin} = i_{dcout} + C_{dcpv}\frac{dV_{dcpv}}{dt}$

i.e. $\frac{dV_{dcpv}}{dt} = \frac{1}{C_{dc}pv}(i_{dcin} - i_{dcout})$ (3.13)

where, $i_{dcin} = (1 - d_{pv})i_{pv}$ is an output current from the DC/DC boost converter and i_{dcout} is an input DC current to the inverter. Here, V_{dcpv} is a voltage across the terminal of the DC-link capacitor.

III. Inverter

The inverter connected between the DC-link capacitor and filter circuit transforms the dc power into ac power with suitable voltage level and frequency. In this project, for modeling the inverter to make it operate as a synchronous generator, the voltage gain model of an inverter

operating in the pulse width modulation (PWM) mode is used. Fig. 3.7 shows the model of an inverter operating in PWM mode.

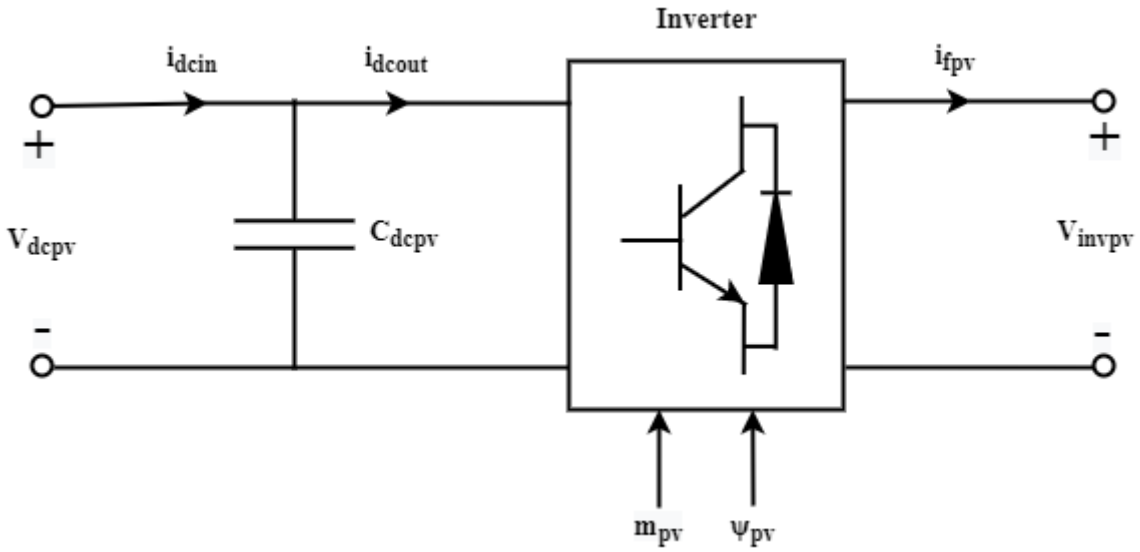

Fig. 3. 7 Inverter circuitry model

Referring fig. 3.7, the power input to the inverter can be expressed as;

$$P_{dcpv} = V_{dcpv} i_{dcout} \tag{3.14}$$

Similarly, the power output of the inverter can be expressed as;

$$P_{acpv} = Re[V_{invpv} i_{fpv}^{*}] \tag{3.15}$$

where, V_{invpv} and i_{fpv} are the output voltage and output current of an inverter respectively.

In d-q axes frame, (3.15) becomes as;

$$V_{invpv} = V_{invdpv} + jV_{invqpv} \tag{3.16}$$

$$i_{fpv} = i_{fdpv} + ji_{fqpv} \tag{3.17}$$

Substituting the values of V_{invpv} and i_{fpv} from (3.16) and (3.17) into (3.15); we get,

$$P_{acpv} = Re[(V_{invdpv} + jV_{invqpv}) \times (i_{fdpv} + ji_{fqpv})^*]$$

i.e. $P_{acpv} = V_{invdpv}i_{fdpv} + V_{invqpv}i_{fqpv}$ (3.18)

Considering the lossless inverter, we can equate (3.14) and (3.18). Hence,

$$P_{dcpv} = P_{acpv}$$

i.e. $V_{dcpv}i_{dcout} = V_{invdpv}i_{fdpv} + V_{invqpv}i_{fqpv}$ (3.19)

As an inverter here is assumed to be operating in PWM mode; the inverter output voltage in terms of DC-link voltage, modulation index m_{pv} and phase angle of the inverter ψ_{pv} can be expressed as;

$$V_{invpv} = m_{pv}V_{dcpv}\angle\psi_{pv} \quad (3.20)$$

In terms of d-q axes;

$$V_{invdpv} = m_{pv}V_{dcpv}\cos(\psi_{pv} + \theta) \quad (3.21)$$

and,

$$V_{invqpv} = m_{pv}V_{dcpv}\sin(\psi_{pv} + \theta) \quad (3.22)$$

Substituting the values of V_{invdpv} and V_{invqpv} from (3.21) and (3.22) into (3.19); we get,

$$i_{dc\text{out}} = m_{pv}i_{fdpv}\cos(\psi_{pv} + \theta) + m_{pv}i_{fqpv}\sin(\psi_{pv} + \theta) \quad (3.23)$$

IV. LCL Filter

In this project, a low bandpass LCL filter is used for attenuating higher-order harmonics received from the inverter. The filter is designed in such a way that the LR section is tapped somewhere in the middle by a capacitor. Here, the inductor allows passing signals with low frequencies and blocks higher frequency harmonics; while a capacitor only allows higher frequency signals to pass and block low frequency harmonics. In this way, these energy-storing

devices incorporate together to deliver ripple free power to the grid [64]. For avoiding the resonance due to the inductor and capacitor in the filter circuitry, a passive damping resistor is added in series to a capacitor.

Now, using KVL in the path starting from the output of the inverter and ending at the damping circuit; we get,

$$V_{invpv} = i_{fpv}R_{fpv} + L_{fpv}\frac{di_{fpv}}{dt} + V_{cpv} + (i_{fpv} - i_{copv})R_{drpv}$$

i.e. $$\frac{di_{fpv}}{dt} = \frac{1}{L_{fpv}}[V_{invpv} - i_{fpv}R_{fpv} - V_{cpv} - (i_{fpv} - i_{copv})R_{drpv}] \quad (3.24)$$

where, R_{fpv}, L_{fpv}, R_{drpv} and V_{cpv} are filter resistance, filter inductance, damping resistance and capacitor voltage of filter respectively.

In terms of d-q axes; (3.24) becomes as;

$$\frac{\boldsymbol{di_{fdpv}}}{\boldsymbol{dt}} = \frac{-\boldsymbol{\omega_0 R_{fpv}}}{\boldsymbol{L_{fpv}}}\boldsymbol{i_{fdpv}} + \boldsymbol{\omega_0 \omega i_{fqpv}} + \frac{\boldsymbol{\omega_0 m_{pv} V_{dcpv}}\cos(\boldsymbol{\psi_{pv}+\theta})}{\boldsymbol{L_{fpv}}} - \frac{\boldsymbol{\omega_0 V_{cdpv}}}{\boldsymbol{L_{fpv}}} - \frac{\boldsymbol{\omega_0 R_{drpv}}}{\boldsymbol{L_{fpv}}}(\boldsymbol{i_{fdpv}} - \boldsymbol{i_{codpv}}) \quad (3.25)$$

and,

$$\frac{\boldsymbol{di_{fqpv}}}{\boldsymbol{dt}} = \frac{-\boldsymbol{\omega_0 R_{fpv}}}{\boldsymbol{L_{fpv}}}\boldsymbol{i_{fqpv}} - \boldsymbol{\omega_0 \omega i_{fdpv}} + \frac{\boldsymbol{\omega_0 m_{pv} V_{dcpv}}\sin(\boldsymbol{\psi_{pv}+\theta})}{\boldsymbol{L_{fpv}}} - \frac{\boldsymbol{\omega_0 V_{cqpv}}}{\boldsymbol{L_{fpv}}} - \frac{\boldsymbol{\omega_0 R_{drpv}}}{\boldsymbol{L_{fpv}}}(\boldsymbol{i_{fqpv}} - \boldsymbol{i_{coqpv}}) \quad (3.26)$$

Similarly, using KVL in the path starting from the microgrid and ending at the damping circuit; we get,

$$V_{cpv} + (i_{fpv} - i_{copv})R_{drpv} = i_{copv}R_{copv} + L_{copv}\frac{di_{copv}}{dt} + V_{mg}$$

i.e. $$\frac{di_{copv}}{dt} = \frac{1}{L_{copv}}[V_{cpv} + (i_{fpv} - i_{copv})R_{drpv} - i_{copv}R_{copv} - V_{mg}] \quad (3.27)$$

In terms of d-q axes; (3.27) becomes as;

$$\frac{di_{codpv}}{dt} = \frac{-\omega_0 R_{copv}}{L_{copv}} i_{codpv} + \omega_0 \omega i_{coqpv} + \frac{\omega_0}{L_{copv}} \left(V_{\mathbf{cdpv}} - V_{\mathbf{mgd}}\right) + \frac{\omega_0 R_{drpv}}{L_{copv}} (i_{fdpv} - i_{codpv}) \quad (3.28)$$

and,

$$\frac{di_{coqpv}}{dt} = \frac{-\omega_0 R_{copv}}{L_{copv}} i_{coqpv} + \omega_0 \omega i_{codpv} + \frac{\omega_0}{L_{copv}} \left(V_{\mathbf{cqpv}} - V_{\mathbf{mgq}}\right) + \frac{\omega_0 R_{drpv}}{L_{copv}} (i_{fqpv} - i_{coqpv}) \quad (3.29)$$

where, R_{copv} and L_{copv} are coupling resistance and inductance of LCL filter respectively.

The current flowing through the filter capacitor is given by;

$$i_{fpv} - i_{copv} = C_{cpv} \frac{dV_{cpv}}{dt}$$

i.e. $\frac{dV_{cpv}}{dt} = \frac{\omega_0}{C_{cpv}} (i_{fpv} - i_{copv})$ (3.30)

where, C_{cpv} is the capacitance of filter.

In terms of d-q axes; (3.30) becomes as;

$$\frac{dV_{cdpv}}{dt} = \frac{\omega_0}{C_{cpv}} \left(i_{fdpv} - i_{codpv}\right) + \omega_0 \omega V_{cqpv} \quad (3.31)$$

and,

$$\frac{dV_{cqpv}}{dt} = \frac{\omega_0}{C_{cpv}} \left(i_{fqpv} - i_{coqpv}\right) - \omega_0 \omega V_{cdpv} \quad (3.32)$$

Thus, the PV system model can be represented by 8 non-linear differential equations (3.12), (3.13), (3.25), (3.26), (3.28), (3.29), (3.31) and (3.32). Hence, the state variables associated with the PV system are;

$$x_{pv} = [i_{pv}, V_{dcpv}, i_{fdpv}, i_{fqpv}, i_{codpv}, i_{coqpv}, V_{cdpv}, V_{cqpv}]^T$$

3.3 Wind Energy Conversion System (WECS)

To form a complete PMSG-based WECS, a sequential combination of gearless drive-train, PMSG, full frequency converter and LCL filter model is used as shown in fig. 3.8. The rotor of a wind turbine placed in an open area couples the rotor of a PMSG by means of a gearless drive-train. As PMSG has its own exciter for field excitation, it not necessarily need any separate exciter for excitation. The stator of the generator is fed to the full-scale converter for getting AC power of constant frequency. The full-scale converter used constitutes of AC/DC rectifier, DC-link capacitor and DC/AC inverter. The AC power of variable frequency received from the stator of PMSG is transformed to DC power with the help of the rectifier. This DC power is stored by the DC-link capacitor at some constant values; which is then converted back to the AC power of suitable frequency by the use of an inverter. As there might be a chance of getting harmonics and ripples at the output side of an inverter, it is further connected to the LCL filter circuitry for getting AC power of desired grid frequency and voltage level.

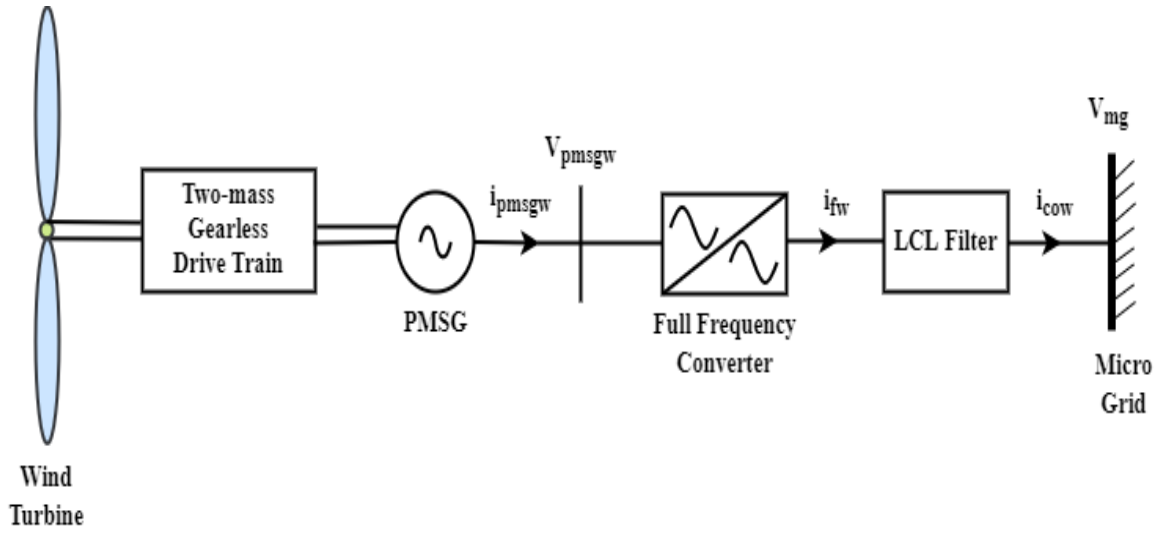

Fig. 3. 8 PMSG based WECS model

3.3.1 Wind Turbine

By utilizing the available wind, blades of wind turbine rotates and generates mechanical power; which is then transferred to the drive-train to run the synchronous generator. The mechanical

power output of the turbine depends on air density, the area swept by the turbine, wind velocity and power coefficient. This mechanical power generated by the wind turbine can be mathematically expressed as;

$$P_{mw} = \frac{1}{2}\rho S V_w^3 C_p(\beta, \lambda) \tag{3.33}$$

where, ρ is the air density, S is the area swept by the turbine, V_w is the wind velocity and $C_P(\beta, \lambda)$ is the power coefficient depending on the tip speed ratio λ and blade pitch angle β.

As the tip speed ratio λ is the ratio of tangential speed of the tip of a blade to the wind velocity; it can be expressed as;

$$\lambda = \frac{\omega_t R}{V_w} \tag{3.34}$$

where, ω_t is the speed of turbine and R is the radius of the blades of a turbine.

Also, the power coefficient $C_P(\beta, \lambda)$ can be expressed in terms of β and λ as;

$$C_P(\beta, \lambda) = 0.5176\left[\frac{116}{\lambda_i} - 0.4\beta - 5\right] e^{-\frac{21}{\lambda_i}} + 0.0068\lambda \tag{3.35}$$

where, $\frac{1}{\lambda_i} = \frac{\beta^3+1-0.035(\lambda+0.08\beta)}{(\lambda+0.08\beta)(\beta^3+1)}$

In this project, a two mass drive-train is used as shown in fig. 3.9. Here, the higher inertial turbine rotor is coupled to the lower inertial PMSG rotor through a drive-train having stiffness of K_s.

The electromechanical equations of such two mass drive-train in terms of torsional angle θ_s and turbine speed ω_t can be expressed as;

$$\frac{d\boldsymbol{\theta_s}}{dt} = \boldsymbol{\omega_0}(\boldsymbol{\omega_t} - \boldsymbol{\omega_w}) \tag{3.36}$$

$$\frac{d\boldsymbol{\omega_t}}{dt} = \frac{\mathbf{1}}{\mathbf{2H_t}}[\boldsymbol{P_{mw}} - \boldsymbol{K_s\theta_s} - \boldsymbol{D_t}(\boldsymbol{\omega_t} - \mathbf{1})] \tag{3.37}$$

where, ω_w is the PMSG rotor speed, H_t is the inertial constant of the turbine and D_t is the damping coefficient of the turbine.

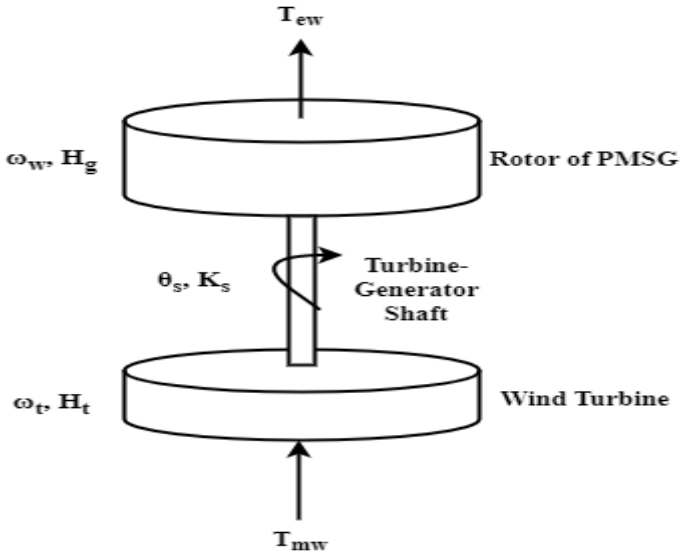

Fig. 3. 9 Two mass drive-train model

3.3.2 Permanent Magnet Synchronous Generator (PMSG)

The equivalent electrical circuit model of PMSG having sinusoidal flux distribution is as shown in fig. 3.10.

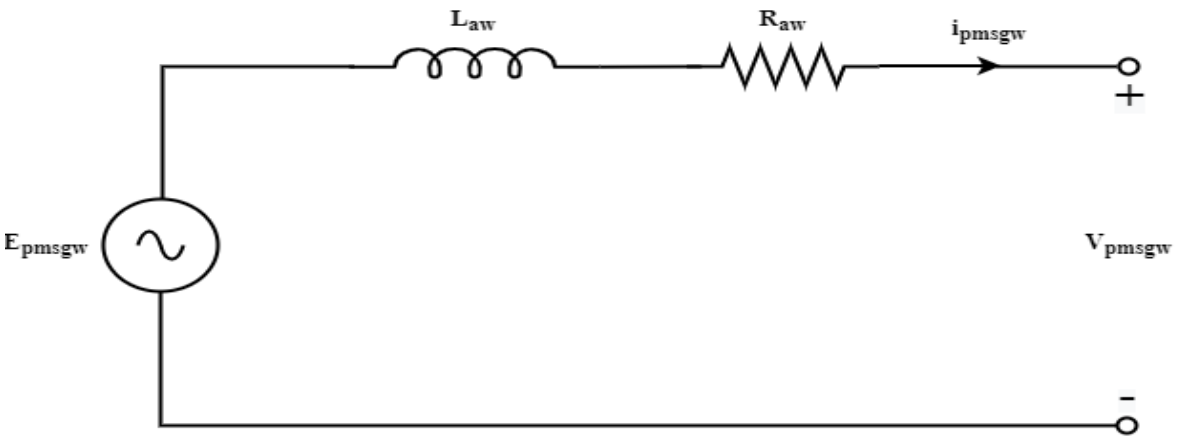

Fig. 3. 10 Equivalent electrical circuit model of PMSG

The d-q axes current-voltage-flux relationship in armature and field circuit of PMSG-based WECS can be expressed as;

$$\psi_{dw} = -X_{dw} i_{pmsgdw} + X_{afdw} i_{fdw} \tag{3.38}$$

$$\psi_{qw} = -X_{qw} i_{pmsgqw} \tag{3.39}$$

$$\psi_{fdw} = -X_{afdw} i_{pmsgdw} + X_{ffdw} i_{fdw} \tag{3.40}$$

Hence, the armature voltage can be decomposed into d-q axes as;

$$\mathrm{V}_{pmsgdw} = -R_{aw} i_{pmsgdw} - \omega_w \psi_{qw} + \frac{1}{\omega_o} \frac{d\psi_{dw}}{dt} \tag{3.41}$$

$$\mathrm{V}_{pmsgqw} = -R_{aw} i_{pmsgqw} + \omega_w \psi_{dw} + \frac{1}{\omega_o} \frac{d\psi_{qw}}{dt} \tag{3.42}$$

As there is permanent magnet in the field for excitation; we can assume that,

$X_{afdw} i_{fdw} = \psi_o$

Hence, (3.41) and (3.42) can be rewritten as;

$$\mathrm{V}_{pmsgdw} = -R_{aw} i_{pmsgdw} + \omega_w \mathrm{X}_{qw} i_{pmsgqw} - \frac{X_{dw}}{\omega_o} \frac{di_{pmsgdw}}{dt}$$

$$\text{i.e. } \frac{\boldsymbol{di_{pmsgdw}}}{\boldsymbol{dt}} = \frac{\boldsymbol{\omega_o}}{\boldsymbol{X_{dw}}} [-\boldsymbol{R_{aw} i_{pmsgdw}} + \boldsymbol{\omega_w} \mathbf{X}_{\boldsymbol{qw}} \boldsymbol{i_{pmsgqw}} - \mathbf{V}_{\boldsymbol{pmsgdw}}] \tag{3.43}$$

and,

$$\mathrm{V}_{pmsgqw} = -R_{aw} i_{pmsgqw} - \omega_w \mathrm{X}_{dw} i_{pmsgdw} + \omega_w \psi_o - \frac{X_{qw}}{\omega_o} \frac{di_{pmsgqw}}{dt}$$

$$\text{i.e. } \frac{\boldsymbol{di_{pmsgqw}}}{\boldsymbol{dt}} = \frac{\boldsymbol{\omega_o}}{\boldsymbol{X_{qw}}} [-\boldsymbol{R_{aw} i_{pmsgqw}} - \boldsymbol{\omega_w} \mathbf{X}_{\boldsymbol{dw}} \boldsymbol{i_{pmsgdw}} + \boldsymbol{\omega_w} \mathbf{E}_{\boldsymbol{fdw}} - \mathbf{V}_{\boldsymbol{pmsgqw}}] \tag{3.44}$$

where, R_{aw} is the armature resistance, X_{dw} and X_{qw} are the armature reactances in d-q axes and E_{fdw} is the field-excitation voltage along d-axis of PMSG-based WECS.

The electromechanical torque produced by the generator can be expressed as;

$$T_{ew} = E_{fdw} i_{pmsgqw} + \left(X_{qw} - X_{dw}\right) i_{pmsgdw} i_{pmsgqw} \tag{3.45}$$

Thus, the power output of the generator becomes as;

$P_{ew} = \omega_w \times T_{ew}$

i.e. $P_{ew} = \omega_w[E_{fdw} i_{pmsgqw} + (X_{qw} - X_{dw}) i_{pmsgdw} i_{pmsgqw}]$ (3.46)

The electromechanical equation of the rotor can be expressed as;

$$\frac{d\delta_w}{dt} = \boldsymbol{\omega_0(\omega_w - 1)} \quad (3.47)$$

and,

$$\frac{d\omega_w}{dt} = \frac{1}{2H_g}[\boldsymbol{K_s\theta_s - P_{ew} - D_g(\omega_w - 1)}] \quad (3.48)$$

where, δ_w is the rotor angle and H_g is the inertial constant of the PMSG.

3.3.3 Full Frequency Converter

As power output of PMSG-based WECS may not be equal to the desired ac power level, it is needed to be converted into the desired level of voltage and frequency before connecting it to the grid. For this, full frequency converter is needed to be employed between the PMSG and the grid. The dominant components used in full frequency converter are AC/DC rectifier (MS converter), DC-link capacitor, DC/AC inverter (GS converter). With this, LCL filter circuitry having coupling inductance is also used at the output terminals of the inverter.

The rectifier connected to the output of the PMSG converts AC into pulsating DC. For keeping this voltage level to remain constant throughout the operation, a DC-link capacitor is used in parallel between the rectifier and an inverter. The dc power stored in the DC-link capacitor is then converted to the ac of required voltage and frequency level by the use of an inverter. But still there might be a chance of getting harmonics and resonance in the power output. In order to reduce it, LCL filter having coupling inductance is incorporated into the system. The

complete model of a PMSG-based WECS with various full frequency converter is presented in fig. 3.11.

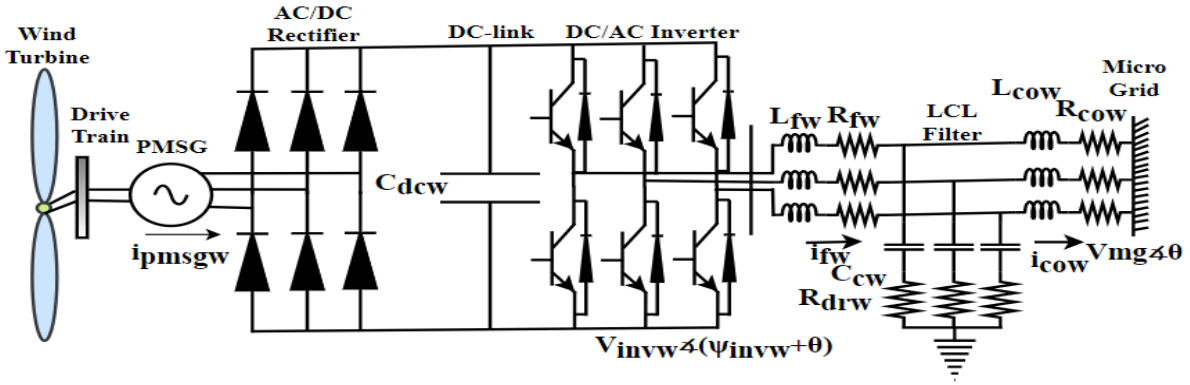

Fig. 3. 11 Interconnection of full frequency converter in a PMSG-based WECS

I. Rectifier or Machine Side (MS) Converter

The voltage at the ac side of the rectifier (i.e. at the output terminal of the PMSG) can be expressed as;

$$V_{pmsgw} = m_{rw}V_{dcw}\angle\alpha \tag{3.49}$$

where, m_{rw} is the modulation index of the rectifier, V_{dcw} is the DC-link voltage, $\alpha = 90^{\circ} - \delta_{rw}$ is the firing angle and δ_{rw} is the rotor angle of the PMSG.

In terms of d-q axes; (3.49) becomes as;

$$V_{pmsgdw} = m_{rw}V_{dcw}\cos(90^{\circ} - \delta_{rw})$$

$$\text{i.e. } V_{pmsgdw} = m_{rw}V_{dcw}\sin\delta_{rw} \tag{3.50}$$

and,

$$V_{pmsgqw} = m_{rw}V_{dcw}\sin(90^{\circ} - \delta_{rw})$$

$$\text{i.e. } V_{pmsgqw} = m_{rw}V_{dcw}\cos\delta_{rw} \tag{3.51}$$

Using (3.50) and (3.51), the power input to the rectifier can be expressed as;

$P_{pmsgw} = V_{pmsgdw} i_{pmsgdw} + V_{pmsgqw} i_{pmsgqw}$

i.e. $P_{pmsgw} = m_{rw} V_{dcw} \sin\delta_{rw} i_{pmsgdw} + m_{rw} V_{dcw} \cos\delta_{rw} i_{pmsgqw}$ (3.52)

II. Inverter or Grid Side (GS) Converter

The output voltage at the ac side of an inverter can be expressed as;

$V_{invw} = m_{invw} V_{dcw} \angle(\psi_{invw} + \theta)$ (3.53)

where, m_{invw} is the modulation index of the inverter, V_{dcw} is the DC-link voltage, $\alpha = \psi_{invw} + \theta$ is the firing angle of the inverter and θ is the phase angle of the microgrid voltage V_{mg}.

In terms of d-q axes; (3.53) becomes as;

$V_{invdw} = m_{invw} V_{dcw} \cos(\psi_{invw} + \theta)$ (3.54)

and,

$V_{invqw} = m_{invw} V_{dcw} \sin(\psi_{invw} + \theta)$ (3.55)

Using (3.54) and (3.55), the power output of the inverter becomes as;

$P_{invw} = V_{invdw} i_{fdw} + V_{invqw} i_{fqw}$

i.e. $P_{invw} = m_{invw} V_{dcw} \cos(\psi_{invw} + \theta) i_{fdw} + m_{invw} V_{dcw} \sin(\psi_{invw} + \theta) i_{fqw}$ (3.56)

III. DC-link Capacitor

The DC-link capacitor by name is an energy storage device linking AC/DC rectifier or MS converter and DC/AC inverter or GS converter. It filters out DC output voltage from the rectifier and helps on ensuring constant voltage at the input side of an inverter.

The power consumed by the DC-link capacitor can be expressed as;

$P_{dcw} = V_{dcw} i_{dcw}$

where, i_{dcw} is the current flowing through the DC-link capacitor and can be expressed as;

$$i_{dcw} = C_{dcw} \frac{dV_{dcw}}{dt}$$

Thus, we get,

$$P_{dcw} = V_{dcw} C_{dcw} \frac{dV_{dcw}}{dt} \tag{3.57}$$

For this case, let us consider the capacitor to be lossless. Thus, we get,

$$P_{dcw} = P_{pmsgw} - P_{invw} \tag{3.58}$$

Using (3.57) and (3.58); we get,

$$V_{dcw} C_{dcw} \frac{dV_{dcw}}{dt} = P_{pmsgw} - P_{invw}$$

i.e. $$\frac{dV_{dcw}}{dt} = \frac{1}{V_{dcw} C_{dcw}} [P_{pmsgw} - P_{invw}] \tag{3.59}$$

Substituting the values of P_{pmsgw} and P_{invw} from (3.52) and (3.56) into (3.59); we get the state equation for the DC-link capacitor as;

i.e. $$\frac{\boldsymbol{dV_{dcw}}}{\boldsymbol{dt}} = \frac{\boldsymbol{1}}{\boldsymbol{C_{dcw}}} [\boldsymbol{m_{rw} \sin\delta_{rw} i_{pmsgdw} + m_{rw} \cos\delta_{rw} i_{pmsgqw} - m_{invw} \cos(\psi_{invw} + \theta) i_{fdw} - m_{invw} \sin(\psi_{invw} + \theta) i_{fqw}}] \tag{3.60}$$

IV. LCL Filter

In this project, for PMSG-based WECS, a low bandpass LCL filter is used for attenuating higher-order harmonics received from the inverter. The filter is designed in such a way that the LR section is tapped somewhere in the middle by a capacitor. Here, the inductor allows to pass signals with low frequencies and blocks higher frequency harmonics; while a capacitor only allows higher frequency signals to pass and blocks low frequency harmonics. In this way, these energy-storing devices incorporate together to deliver ripple free power to the grid [64]. For avoiding the resonance due to the inductor and capacitor in the filter circuitry, a passive damping resistor is added in series to a capacitor.

Now, using KVL in the path starting from the output of the inverter and ending at the damping circuit; we get,

$$V_{invw} = i_{fw}R_{fw} + L_{fw}\frac{di_{fw}}{dt} + V_{cw} + (i_{fw} - i_{cow})R_{drw}$$

i.e. $$\frac{di_{fw}}{dt} = \frac{1}{L_{fw}}[V_{invw} - i_{fw}R_{fw} - V_{cw} - (i_{fw} - i_{cow})R_{drw}] \quad (3.61)$$

where, R_{fw}, L_{fw}, R_{drw} and V_{cw} are filter resistance, filter inductance, damping resistance and capacitor voltage of filter respectively.

In terms of d-q axes; (3.61) becomes as;

$$\frac{\boldsymbol{di_{fdw}}}{\boldsymbol{dt}} = \frac{\boldsymbol{-\omega_0 R_{fw}}}{\boldsymbol{L_{fw}}}\boldsymbol{i_{fdw}} + \boldsymbol{\omega_0 \omega i_{fqw}} + \frac{\boldsymbol{\omega_0 m_{invw} V_{dcw}\cos(\psi_{invw}+\theta)}}{\boldsymbol{L_{fw}}} - \frac{\boldsymbol{\omega_0 V_{cdw}}}{\boldsymbol{L_{fw}}} - \frac{\boldsymbol{\omega_0 R_{drw}}}{\boldsymbol{L_{fw}}}(\boldsymbol{i_{fdw} - i_{codw}})$$

(3.62)

and,

$$\frac{\boldsymbol{di_{fqw}}}{\boldsymbol{dt}} = \frac{\boldsymbol{-\omega_0 R_{fw}}}{\boldsymbol{L_{fw}}}\boldsymbol{i_{fqw}} - \boldsymbol{\omega_0 \omega i_{fdw}} + \frac{\boldsymbol{\omega_0 m_{invw} V_{dcw}\sin(\psi_{invw}+\theta)}}{\boldsymbol{L_{fw}}} - \frac{\boldsymbol{\omega_0 V_{cqw}}}{\boldsymbol{L_{fw}}} - \frac{\boldsymbol{\omega_0 R_{drw}}}{\boldsymbol{L_{fw}}}(\boldsymbol{i_{fqw} - i_{coqw}})$$

(3.63)

Similarly, using KVL in the path starting from the microgrid and ending at the damping circuit; we get,

$$V_{cw} + (i_{fw} - i_{cow})R_{drw} = i_{cow}R_{cow} + L_{cow}\frac{di_{cow}}{dt} + V_{mg}$$

i.e. $$\frac{di_{cow}}{dt} = \frac{1}{L_{cow}}[V_{cw} + (i_{fw} - i_{cow})R_{drw} - i_{cow}R_{cow} - V_{mg}] \quad (3.64)$$

In terms of d-q axes; (3.64) becomes as;

$$\frac{\boldsymbol{di_{codw}}}{\boldsymbol{dt}} = \frac{\boldsymbol{-\omega_0 R_{cow}}}{\boldsymbol{L_{cow}}}\boldsymbol{i_{codw}} + \boldsymbol{\omega_0 \omega i_{coqw}} + \frac{\boldsymbol{\omega_0}}{\boldsymbol{L_{cow}}}(\boldsymbol{V_{cdw} - V_{mgd}}) + \frac{\boldsymbol{\omega_0 R_{drw}}}{\boldsymbol{L_{cow}}}(\boldsymbol{i_{fdw} - i_{codw}}) \quad (3.65)$$

and,

$$\frac{di_{coqw}}{dt} = \frac{-\omega_0 R_{cow}}{L_{cow}} i_{coqw} + \omega_0 \omega i_{codw} + \frac{\omega_0}{L_{cow}} \left(V_{\mathrm{cqw}} - V_{\mathrm{mgq}}\right) + \frac{\omega_0 R_{drw}}{L_{cow}} (i_{fqw} - i_{coqw}) \quad (3.66)$$

where, R_{cow} and L_{cow} are coupling resistance and inductance of LCL filter respectively.

The current flowing through the filter capacitor is given by;

$$i_{fw} - i_{cow} = C_{cw} \frac{dV_{cw}}{dt}$$

i.e. $$\frac{dV_{cw}}{dt} = \frac{\omega_0}{C_{cw}} (i_{fw} - i_{cow}) \quad (3.67)$$

where, C_{cw} is the capacitance of filter.

In terms of d-q axes; (3.67) becomes as;

$$\frac{dV_{cdw}}{dt} = \frac{\omega_0}{C_{cw}} \left(i_{fdw} - i_{codw}\right) + \omega_0 \omega V_{cqw} \quad (3.68)$$

and,

$$\frac{dV_{cqw}}{dt} = \frac{\omega_0}{C_{cw}} \left(i_{fqw} - i_{coqw}\right) - \omega_0 \omega V_{cdw} \quad (3.69)$$

Thus, the PMSG-based WECS model can be represented by 13 non-linear differential equations (3.36), (3.37), (3.43), (3.44), (3.47), (3.48), (3.60), (3.62), (3.63), (3.65), (3.66), (3.68) and (3.69). Hence, the state variables associated with the PMSG-based WECS are;

$$x_w = [\theta_s, \omega_t, \delta_w, \omega_w, i_{pmsgdw}, i_{pmsgqw}, V_{dcw}, i_{fdw}, i_{fqw}, i_{codw}, i_{coqw}, V_{cdw}, V_{cqw}]^T$$

3.4 Microalternator System

The microalternator used in this project can be modeled as a synchronous generator as they can directly be coupled to the grid. Thus, the microalterator can be represented by the fourth order model consisting of the swing equation, internal voltage equation and field voltage along d-axis [39].

The rotor of the microalternator can be represented by the swing equation as;

$$\frac{2H_a}{\omega_o}\frac{d^2\delta_a}{dt^2} = P_{ma} - P_{ea} - D_a(\omega_a - \omega_o) \tag{3.70}$$

where, H_a is the inertial constant of the rotor, δ_a is the rotor angle, ω_a is the rotor speed, D_a is the damping coefficient, P_{ma} is the mechanical power input and P_{ea} is the electrical power output of the microalternator.

On decomposing (3.70) into two first order differential equations; we get,

$$\boldsymbol{\frac{d\delta_a}{dt} = \omega_o(\omega_a - 1)} \tag{3.71}$$

and,

$$\boldsymbol{\frac{d\omega_a}{dt} = \frac{1}{2Ha}[P_{ma} - P_{ea} - D_a(\omega_a - \omega_o)]} \tag{3.72}$$

The internal voltage $e_q{}'$ of the generator can be expressed as;

$$\boldsymbol{\frac{de_q{}'}{dt} = \frac{1}{T_{do}{}'}\left[E_{fd} - e_q{}' - (x_{da} - x'_{da})i_{tda}\right]} \tag{3.73}$$

where, x_{da} is the d-axis synchronous reactance, x'_{da} is the d-axis transient reactance and T'_{do} is the open-circuit field constant of the microalternator.

The field voltage along d-axis can be expressed as;

$$\boldsymbol{\frac{dE_{fd}}{dt} = \frac{1}{T_a}[K_a(V_{tref} - V_t) - (E_{fd} - E_{fdo})\ ]} \tag{3.74}$$

where, K_a is the gain and T_a is the time constant of the exciter.

Thus, the microalternator system can be represented by 4 non-linear differential equations (3.71), (3.72), (3.73) and (3.74). Hence, the state variables associated with the microalternator are;

$$\boldsymbol{x_a = [\delta_a, \omega_a, e_q', E_{fd}]^T}$$

Let us consider that the microalternator is connected to the microgrid for both autonomous and non-autonomous modes as shown in fig. 3.12.

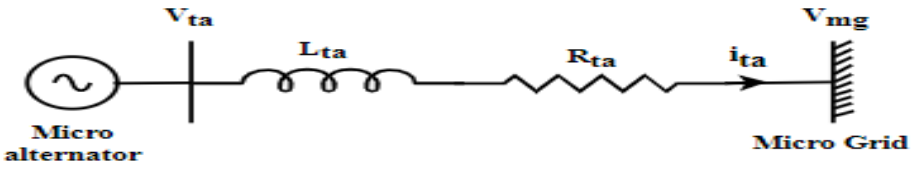

Fig. 3. 12 Microalternator interfaced to the microgrid

Using KVL between the terminal of microalternator and microgrid; we get,

$$V_{ta} = (R_{ta} + jx_{ta})i_{ta} + V_{mg}$$

where, $x_{ta} = L_{ta}\omega_a$ is the reactance of the line.

$$i_{ta} = i_{tda} + ji_{tqa}$$

$$V_{mg} = V_{dmg} + jV_{qmg}$$

i.e. $V_{ta} = (R_{ta} + jx_{ta})(i_{tda} + ji_{tqa}) + (V_{dmg} + jV_{qmg})$

i.e. $V_{ta} = (V_{dmg} + R_{ta}i_{tda} - x_{ta}i_{tqa}) + j(V_{qmg} + R_{ta}i_{tqa} + x_{ta}i_{tda})$ (3.75)

In d-q axes; the terminal voltage of the microalternator can be expressed as;

$$V_{ta} = V_{tda} + jV_{tqa}$$

where, $V_{tda} = x_{qa}i_{tqa}$

$$V_{tqa} = e_q' - x_{da}'i_{tda}$$

i.e. $V_{ta} = x_{qa}i_{tqa} + j(e_q' - x_{da}'i_{tda})$ (3.76)

Thus, from (3.75) and (3.76); we get,

$$(V_{dmg} + R_{ta}i_{tda} - x_{ta}i_{tqa}) + j(V_{qmg} + R_{ta}i_{tqa} + x_{ta}i_{tda}) = x_{qa}i_{tqa} + j(e_q{}' - x_{da}{}'i_{tda})$$

On equating real and imaginary parts; we get,

$$x_{qa}i_{tqa} = V_{dmg} + R_{ta}i_{tda} - x_{ta}i_{tqa}$$

i.e. $(x_{qa} + x_{ta})i_{tqa} - R_{ta}i_{tda} = V_{dmg}$ (3.77)

and,

$$e_q{}' - x_{da}{}'i_{tda} = V_{qmg} + R_{ta}i_{tqa} + x_{ta}i_{tda}$$

i.e. $R_{ta}i_{tqa} + (x_{da}{}' + x_{ta})i_{tda} = e_q{}' - V_{qmg}$ (3.78)

On solving (3.77) and (3.78); we get,

$$i_{tda} = \frac{-R_{ta}V_{dmg} + (e_q{}' - V_{qmg})(x_{qa} + x_{ta})}{R_{ta}{}^2 + (x_{da}{}' + x_{ta})(x_{qa} + x_{ta})} \quad (3.79)$$

and,

$$i_{tqa} = \frac{V_{dmg}(x'_{da} + x_{ta})(x_{qa} + x_{ta}) + R_{ta}(e_q{}' - V_{qmg})(x_{qa} + x_{ta})}{(x_{qa} + x_{ta})[R_{ta}{}^2 + (x_{da}{}' + x_{ta})(x_{qa} + x_{ta})]} \quad (3.80)$$

The terminal voltage of the microalternator can be expressed as;

$$V_{ta} = \sqrt{V_{tda}^2 + V_{tqa}^2}$$

i.e. $V_{ta} = \sqrt{(x_{qa}i_{tqa})^2 + (e_q{}' - x_{da}{}'i_{tda})^2}$ (3.81)

The mathematical expression for the electrical power output can be written as;

$$P_{ea} = V_{tda}i_{tda} + V_{tqa}i_{tqa}$$

i.e. $P_{ea} = (x_{qa}i_{tqa})i_{tda} + (e_q{}' - x_{da}{}'i_{tda})i_{tqa}$

i.e. $P_{ea} = (e_q{}'i_{tqa}) + (x_{qa} - x_{da}{}')i_{tda}i_{tqa}$ (3.82)

On substituting (3.79) and (3.80) into (3.81) and (3.82); we can get the terminal voltage and power output of the microalternator in terms of microgrid voltage components V_{dmg} and V_{qmg}.

3.5 Static Synchronous Compensator (STATCOM)

The STATCOM with capacitor energy storage system is used in this project for regulating the system voltage and frequency. The STATCOM fulfills the reactive power demand of the system while the capacitor energy storage system fulfills the active power demand of the system for a short time.

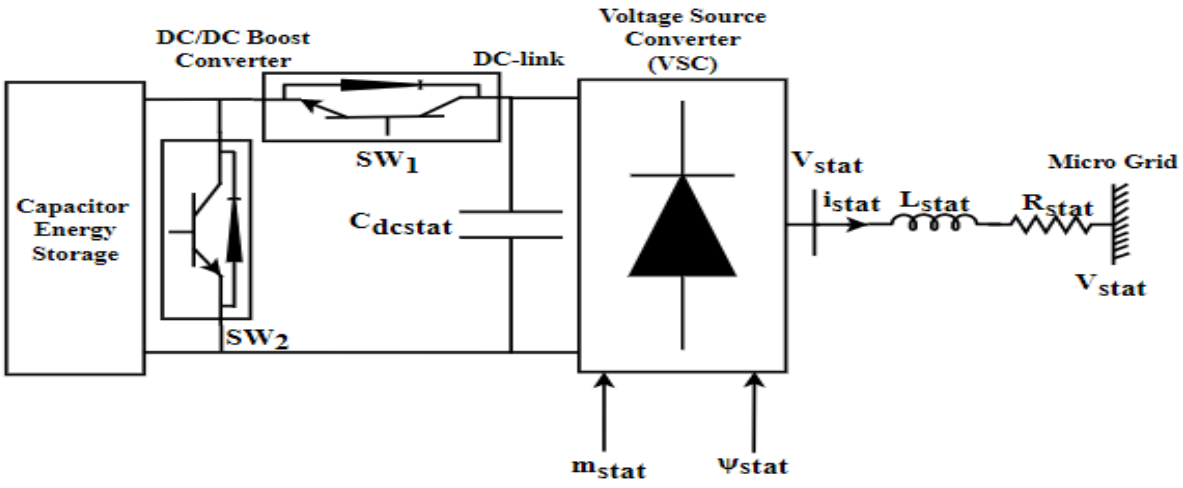

Fig. 3. 13 Central controller model

Fig. 3.13 shows the STATCOM with capacitor energy storage device as a central controller. Here, the STATCOM is modeled as a voltage source converter (VSC) and is capable of supplying reactive power by changing the modulation index (m_{stat}) of the controller. Similarly, the energy storage device delivers active power by changing the phase angle (ψ_{stat}) of the converter.

Using KVL at the output side of the STATCOM; we get,

$$V_{stat} - V_{mg} = L_{stat}\frac{di_{stat}}{dt} + R_{stat}i_{stat}$$

i.e. $\frac{di_{stat}}{dt} = \frac{1}{L_{stat}}[-R_{stat}i_{stat} + V_{stat} - V_{mg}]$ (3.83)

where, R_{stat} is the resistance, L_{stat} is the inductance, V_{stat} is the output voltage and i_{stat} is the output current of the STATCOM.

The output voltage of the STATCOM can be expressed as;

$$V_{stat} = m_{stat} V_{dcstat} \angle(\psi_{stat} + \theta) \tag{3.84}$$

where, m_{stat} is the modulation index, V_{dcstat} is the DC-link voltage, $\alpha = \psi_{stat} + \theta$ is the firing angle of the STATCOM and θ is the phase angle of the microgrid voltage V_{mg}.

In terms of d-q axes; (3.84) becomes as;

$$V_{dstat} = m_{stat} V_{dcstat} \cos(\psi_{stat} + \theta) \tag{3.85}$$

and,

$$V_{qstat} = m_{stat} V_{dcstat} \sin(\psi_{stat} + \theta) \tag{3.86}$$

Using (3.85) and (3.86) after expressing (3.83) in terms of d-q axes; we get,

$$\frac{di_{dstat}}{dt} = \frac{-\omega_0 R_{stat}}{L_{stat}} i_{dstat} + \omega_0 \omega i_{qstat} + \frac{\omega_0 m_{stat} V_{dcstat} \cos(\psi_{stat}+\theta)}{L_{stat}} - \frac{\omega_0 V_{dstat}}{L_{stat}} \tag{3.87}$$

and,

$$\frac{di_{qstat}}{dt} = \frac{-\omega_0 R_{stat}}{L_{stat}} i_{qstat} - \omega_0 \omega i_{dstat} + \frac{\omega_0 m_{stat} V_{dcstat} \sin(\psi_{stat}+\theta)}{L_{stat}} - \frac{\omega_0 V_{qstat}}{L_{stat}} \tag{3.88}$$

The current output of the storage capacitor (i_{dcs}) is given by;

$$i_{dcs} = C_{dcstat} \frac{dE_s}{dt} \tag{3.89}$$

where, C_{dcstat} is the capacitance of storage capacitor and E_s is the voltage of the capacitor.

Using KCL at the DC-link; we get,

$$i_{dcstat} - i_{dcs} = C_{dcstat} \frac{dV_{dcstat}}{dt}$$

i.e. $\frac{dV_{dcstat}}{dt} = \frac{1}{C_{dcstat}}[i_{dcstat} - i_{dcs}]$ (3.90)

where, V_{dcstat} is the DC-link voltage and i_{dcstat} is the DC-link current of the STATCOM.

Let us consider the controller to be lossless. In such a case, the power input and output of the STATCOM needs to be equal in magnitude. Hence,

$P_{dcstat} = P_{acstat}$

i.e. $i_{dcs}V_{dcstat} = V_{stat}i_{stat}$ (3.91)

In terms of d-q axes; (3.91) becomes as;

$i_{dcs}V_{dcstat} = V_{dstat}i_{dstat} + V_{qstat}i_{qstat}$ (3.92)

Using (3.85) and (3.86) into (3.92); we get,

$i_{dcs}V_{dcstat} = [m_{stat}V_{dcstat}\cos(\psi_{stat} + \theta)]i_{dstat} + [m_{stat}V_{dcstat}\sin(\psi_{stat} + \theta)]i_{qstat}$

i.e. $i_{dcs} = m_{stat}i_{dstat}\cos(\psi_{stat} + \theta) + m_{stat}i_{qstat}\sin(\psi_{stat} + \theta)$ (3.93)

Substituting (3.93) into (3.90); we get,

$$\frac{\boldsymbol{dV_{dcstat}}}{\boldsymbol{dt}} = \frac{\boldsymbol{1}}{\boldsymbol{C_{dcstat}}}\left[\boldsymbol{i_{dcstat}} - \{\boldsymbol{m_{stat}i_{dstat}}\mathbf{cos}(\boldsymbol{\psi_{stat}} + \boldsymbol{\theta}) + \boldsymbol{m_{stat}i_{qstat}}\mathbf{sin}(\boldsymbol{\psi_{stat}} + \boldsymbol{\theta})\}\right] \quad (3.94)$$

Thus, the central controller system with STATCOM and capacitor energy storage can be represented by 3 non-linear differential equations (3.87), (3.88) and (3.94). Hence, the state variables associated with the STATCOM are;

$$\boldsymbol{x_{stat}} = [\boldsymbol{i_{dstat}}, \boldsymbol{i_{qstat}}, \boldsymbol{V_{dcstat}}]^{\boldsymbol{T}}$$

Chapter 4

Microgrid System Composite Model

In this chapter, different components of microgrid considered in this project; i.e. photovoltaic (PV), wind energy conversion system (WECS), microalternator and static synchronous compensator (STATCOM) modeled by the non-linear differential equations are combined together to form a common microgrid system capable of operating in both autonomous and non-autonomous modes.

Fig. 4.1 presents the overall circuitry diagram of the microgrid model. The PV, WECS, microalternator, STATCOM and load are connected together at the point of common coupling (PCC). Here, as microalternator behaves as a synchronous generator and is capable of generating ac power of required voltage and frequency level, it is connected directly to the PCC without any intermediate converter; while the PV and PMSG are interfaced to the PCC via power conditioning unit (PCU) and full frequency converter respectively. Additionally, LCL filter circuitry is also included between the generating sources and the PCC for getting the desired ac power at constant level of voltage and frequency. For active and reactive power support at the time of temporary disturbances or during the disconnection of the grid, STATCOM with capacitor energy storage system is also connected to the grid. The combination of all these power generating units and compensator supplies power to the constant power loads. In case of non-autonomous mode of operation, power if excess may be transmitted to the main grid as shown by the arrow-head 'i_g' in the figure.

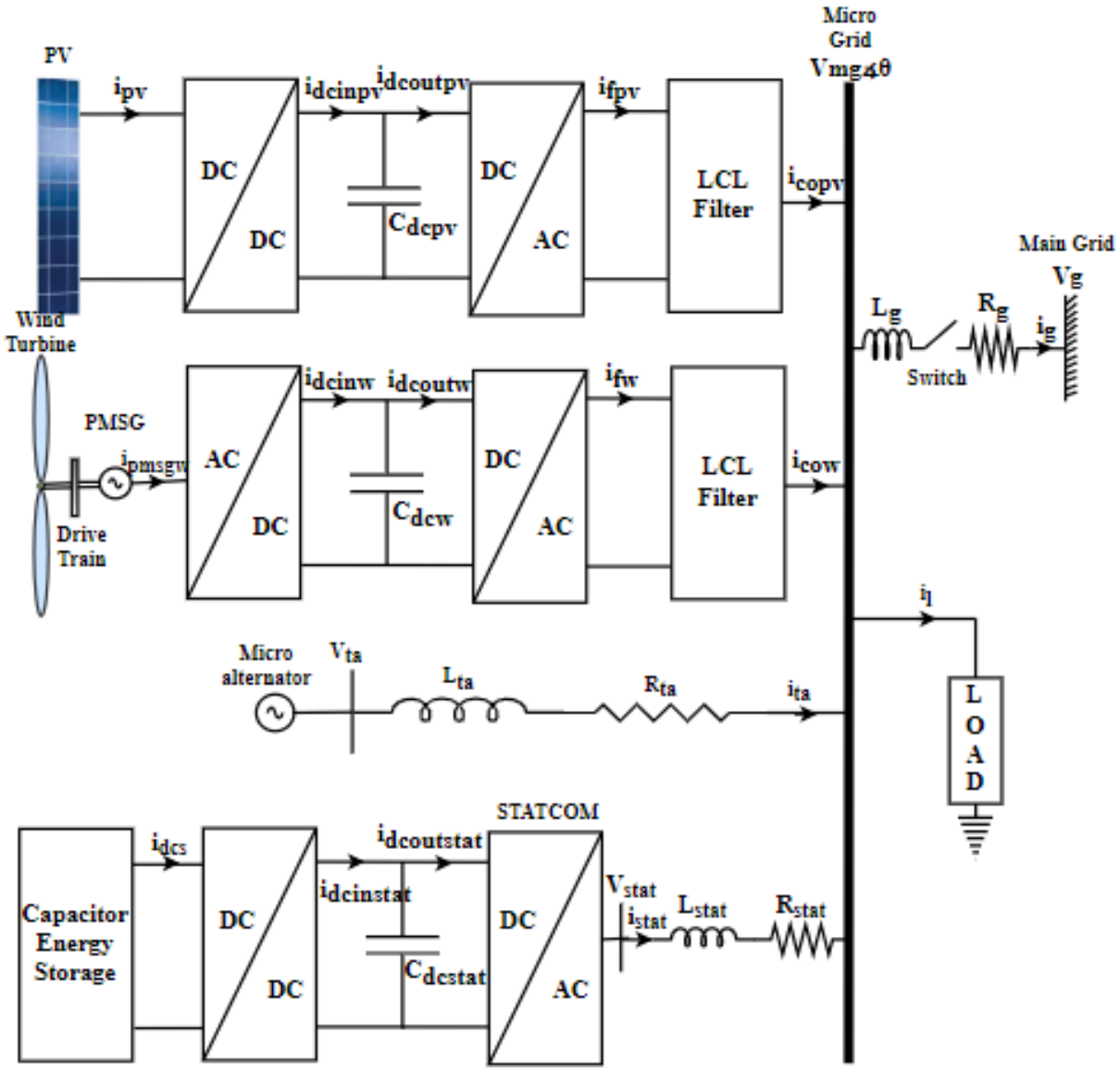

Fig. 4. 1 Microgrid system model for both autonomous and non-autonomous modes of operation

4.1 Non-Autonomous Mode of Operation

Applying KCL at the PCC; we get,

$$i_{copv} + i_{cow} + i_{ta} + i_{stat} = i_l + i_g \tag{4.1}$$

In terms of d-q axes; (4.1) becomes as;

$$i_{codpv} + i_{codw} + i_{tda} + i_{dstat} = i_{dl} + i_{dg} \tag{4.2}$$

and,

$$i_{coqpv} + i_{coqw} + i_{tqa} + i_{qstat} = i_{ql} + i_{qg} \tag{4.3}$$

Let us model the load at the PCC by an admittance $Y = g - jb$. The load current then can be expressed as;

$i_l = V_{mg}Y$

i.e. $i_l = V_{mg}(g - jb)$ (4.4)

In terms of d-q axes; (4.4) becomes as;

$i_{dl} + ji_{ql} = (V_{dmg} + jV_{qmg})(g - jb)$

i.e. $i_{dl} + ji_{ql} = gV_{dmg} - jbV_{dmg} + jgV_{qmg} + bV_{qmg}$

i.e. $i_{dl} + ji_{ql} = (gV_{dmg} + bV_{dmg}) + j(gV_{qmg} - bV_{dmg})$ (4.5)

Equating real and imaginary parts; we get,

$i_{dl} = gV_{dmg} + bV_{dmg}$ (4.6)

and,

$i_{ql} = gV_{qmg} - bV_{dmg}$ (4.7)

The current flowing from PCC to the main grid can be written as;

$i_g = \frac{V_{mg} - V_g}{R_g + jX_g}$ (4.8)

In terms of d-q axes; we get,

$i_{dg} + ji_{qg} = \frac{(V_{dmg} + jV_{qmg}) - (V_g sin\delta_a + jV_g cos\delta_a)}{R_g + jX_g}$

i.e. $i_{dg} + ji_{qg} = \frac{[(V_{dmg} - V_g sin\delta_a) + j(V_{qmg} - V_g cos\delta_a)](R_g - jX_g)}{(R_g)^2 - (jX_g)^2}$

i.e. $i_{dg} + ji_{qg} = \frac{R_g(V_{dmg} - V_g sin\delta_a) + X_g(V_{qmg} - V_g cos\delta_a) + jR_g(V_{qmg} - V_g cos\delta_a) - jX_g(V_{dmg} - V_g sin\delta_a)}{{R_g}^2 + {X_g}^2}$

Equating real and imaginary parts; we get,

$$i_{dg} = \frac{R_g(V_{dmg} - V_g sin\delta_a) + X_g(V_{qmg} - V_g cos\delta_a)}{{R_g}^2 + {X_g}^2} \quad (4.9)$$

and,

$$i_{qg} = \frac{R_g(V_{qmg} - V_g cos\delta_a) - X_g(V_{dmg} - V_g sin\delta_a)}{{R_g}^2 + {X_g}^2} \quad (4.10)$$

Substituting the values of i_{tda}, i_{dl} and i_{dg} from (3.79), (4.6) and (4.9) respectively into (4.2); we get,

$$i_{codpv} + i_{codw} + \frac{-R_{ta}V_{dmg} + ({e_q}' - V_{qmg})(x_{qa} + x_{ta})}{{R_{ta}}^2 + (x_{da}' + x_{ta})(x_{qa} + x_{ta})} + i_{dstat} = (gV_{dmg} + bV_{dmg}) +$$

$$\frac{R_g(V_{dmg} - V_g sin\delta_a) + X_g(V_{qmg} - V_g cos\delta_a)}{{R_g}^2 + {X_g}^2} \quad (4.11)$$

Let; $X_1 = {x_{da}}' + x_{ta}$

$X_2 = x_{qa} + x_{ta}$

$Z_1 = {R_{ta}}^2 + X_1X_2$

$Z_g = {R_g}^2 + {X_g}^2$

Using these variables in (4.11); we get,

$$i_{codpv} + i_{codw} + \frac{-R_{ta}V_{dmg} + ({e_q}' - V_{qmg})X_2}{Z_1} + i_{dstat} = (gV_{dmg} + bV_{dmg}) +$$

$$\frac{R_g(V_{dmg} - V_g sin\delta_a) + X_g(V_{qmg} - V_g cos\delta_a)}{Z_g}$$

i.e.$Z_gZ_1(i_{codpv} + i_{codw} + i_{dstat}) - R_{ta}Z_gV_{dmg} + Z_gX_2{e_q}' - Z_gX_2V_{qmg} = gZ_gZ_1V_{dmg} +$

$bZ_gZ_1V_{qmg} + Z_1R_gV_{dmg} - Z_1R_gV_g sin\delta_a + Z_1X_gV_{qmg} - Z_1X_gV_g cos\delta_a$

i.e.$(gZ_gZ_1 + Z_1R_g + Z_gR_{ta})V_{dmg} + (bZ_gZ_1 + Z_1X_g + Z_gX_2)V_{qmg} = Z_gZ_1(i_{codpv} +$

$i_{codw} + i_{dstat}) + Z_gX_2{e_q}' + Z_1X_gV_g cos\delta_a + Z_1R_gV_g sin\delta_a \quad (4.12)$

Similarly, substituting the values of i_{tqa}, i_{ql} and i_{qg} from (3.80), (4.7) and (4.10) respectively into (4.3); we get,

$$i_{coqpv} + i_{coqw} + \frac{V_{dmg}(x'_{da}+x_{ta})(x_{qa}+x_{ta})+R_{ta}(e_q{}'-V_{qmg})(x_{qa}+x_{ta})}{(x_{qa}+x_{ta})[R_{ta}{}^2+(x_{da}{}'+x_{ta})(x_{qa}+x_{ta})]} + i_{qstat} = (gV_{qmg} - bV_{dmg}) +$$

$$\frac{R_g(V_{qmg}-V_g cos\delta_a)-X_g(V_{dmg}-V_g sin\delta_a)}{R_g{}^2+X_g{}^2} \quad (4.13)$$

In terms of X_1, X_2, Z_1 and Z_g as in the case of d-axes current; (4.13) becomes as;

$$i_{coqpv} + i_{coqw} + \frac{X_1X_2V_{dmg}+R_{ta}(e_q{}'-V_{qmg})X_2}{Z_1X_2} + i_{qstat} = (gV_{qmg} - bV_{dmg}) +$$

$$\frac{R_g(V_{qmg}-V_g cos\delta_a)-X_g(V_{dmg}-V_g sin\delta_a)}{Z_g}$$

i.e.$Z_gZ_1X_2(i_{coqpv} + i_{coqw} + i_{qstat}) + Z_gX_1X_2V_{dmg} + Z_gX_2R_{ta}e_q{}' - Z_gX_2R_{ta}V_{qmg} =$

$gZ_gZ_1X_2V_{qmg} - bZ_gZ_1X_2V_{dmg} + Z_1X_2R_gV_{qmg} - Z_1X_2R_gV_g cos\delta_a - Z_1X_gX_2V_{dmg} +$

$Z_1X_gX_2V_g sin\delta_a$

i.e.$(bZ_gZ_1X_2 + Z_1X_gX_2 + Z_gX_1X_2)V_{dmg} - (gZ_gZ_1X_2 + Z_1X_2R_g + Z_gX_2R_{ta})V_{qmg} =$

$-Z_gZ_1X_2(i_{coqpv} + i_{coqw} + i_{qstat}) - Z_gX_2R_{ta}e_q{}' - Z_1X_2R_gV_g cos\delta_a + Z_1X_gX_2V_g sin\delta_a$(4.14)

Let (4.12) and (4.13) be expressed as;

$$AV_{dmg} + BV_{qmg} = Z_gZ_1(i_{codpv} + i_{codw} + i_{dstat}) + Z_gX_2e_q{}' + Z_1V_g(R_g sin\delta_a + X_g cos\delta_a)$$

i.e.$V_{dmg} = \frac{1}{A}[Z_gZ_1(i_{codpv} + i_{codw} + i_{dstat}) + Z_gX_2e_q{}' + Z_1V_g(R_g sin\delta_a + X_g cos\delta_a) -$

$BV_{qmg}]$ (4.15)

and,

$$CV_{dmg} - AX_2V_{qmg} = -Z_gZ_1X_2(i_{coqpv} + i_{coqw} + i_{qstat}) - Z_gX_2R_{ta}e_q{}' -$$

$$Z_1X_2V_g(R_g cos\delta_a - X_g sin\delta_a) \quad (4.16)$$

where,

$A = gZ_gZ_1 + Z_1R_g + Z_gR_{ta}$

$B = bZ_gZ_1 + Z_1X_g + Z_gX_2$

$C = bZ_gZ_1X_2 + Z_1X_gX_2 + Z_gX_1X_2$

Putting the values of V_{dmg} from (4.15) into (4.16); we get,

$C \times \frac{1}{A}[Z_gZ_1(i_{codpv} + i_{codw} + i_{dstat}) + Z_gX_2e_q' + Z_1V_g(R_gsin\delta_a + X_gcos\delta_a) - BV_{qmg}] - AX_2V_{qmg} = -Z_gZ_1X_2(i_{coqpv} + i_{coqw} + i_{qstat}) - Z_gX_2R_{ta}e_q' - Z_1X_2V_g(R_gcos\delta_a - X_gsin\delta_a)$

i.e. $\frac{C}{A}Z_gZ_1(i_{codpv} + i_{codw} + i_{dstat}) + \frac{C}{A}Z_gX_2e_q' + \frac{C}{A}Z_1R_gV_gsin\delta_a + \frac{C}{A}Z_1X_gV_gcos\delta_a - \frac{BC}{A}V_{qmg} - AX_2V_{qmg} = -Z_gZ_1X_2(i_{coqpv} + i_{coqw} + i_{qstat}) - Z_gX_2R_{ta}e_q' - Z_1X_2R_gV_gcos\delta_a + Z_1X_gX_2V_gsin\delta_a$

i.e. $\frac{C}{A}Z_gZ_1(i_{codpv} + i_{codw} + i_{dstat}) + (\frac{C}{A} + R_{ta})Z_gX_2e_q' + Z_gZ_1X_2(i_{coqpv} + i_{coqw} + i_{qstat}) + (\frac{C}{A}Z_1R_g - Z_1X_gX_2)V_gsin\delta_a + (\frac{C}{A}Z_1X_g + Z_1X_2R_g)V_gcos\delta_a - (\frac{BC}{A} + AX_2)V_{qmg} = 0$

i.e. $\left(\frac{BC+A^2X_2}{A}\right)V_{qmg} = \frac{C}{A}Z_gZ_1(i_{codpv} + i_{codw} + i_{dstat}) + \left(\frac{C+AR_{ta}}{A}\right)Z_gX_2e_q' + Z_gZ_1X_2(i_{coqpv} + i_{coqw} + i_{qstat}) + \left(\frac{CZ_1R_g - AZ_1X_gX_2}{A}\right)V_gsin\delta_a + \left(\frac{CZ_1X_g + AZ_1X_2R_g}{A}\right)V_gcos\delta_a$

i.e. $V_{qmg} = \frac{1}{BC+A^2X_2}[CZ_gZ_1(i_{codpv} + i_{codw} + i_{dstat}) + (C + AR_{ta})Z_gX_2e_q' + AZ_gZ_1X_2(i_{coqpv} + i_{coqw} + i_{qstat}) + (CZ_1R_g - AZ_1X_gX_2)V_gsin\delta_a + (CZ_1X_g + AZ_1X_2R_g)V_gcos\delta_a]$

Let; $BC + A^2X_2 = Den$

So,$V_{qmg} = \frac{1}{Den} CZ_g Z_1 \left(i_{codpv} + i_{codw} + i_{dstat}\right) + \frac{1}{Den} (CZ_g X_2 +$

$AZ_g X_2 R_{ta}) e_q' + \frac{1}{Den} AZ_g Z_1 X_2 \left(i_{coqpv} + i_{coqw} + i_{qstat}\right) + \frac{1}{Den} [\left(CZ_1 X_g + AZ_1 X_2 R_g\right) cos\delta_a +$

$(CZ_1 R_g - AZ_1 X_g X_2) sin\delta_a] V_g$

i.e. $V_{qmg} = D\left(i_{codpv} + i_{codw} + i_{dstat}\right) + Ee_q' + F\left(i_{coqpv} + i_{coqw} + i_{qstat}\right) + GV_g$ (4.17)

where,

$$D = \frac{1}{Den} CZ_g Z_1$$

$$E = \frac{1}{Den} (CZ_g X_2 + AZ_g X_2 R_{ta})$$

$$F = \frac{1}{Den} AZ_g Z_1 X_2$$

$$G = \frac{1}{Den} [\left(CZ_1 X_g + AZ_1 X_2 R_g\right) cos\delta_a + (CZ_1 R_g - AZ_1 X_g X_2) sin\delta_a]$$

Using these values; V_{dmg} and V_{qmg} can be determined while operating non-autonomous mode; and then can be used in the state equations of different component models. Thus, the state equation takes the form of;

$$\dot{X} = f(X, u)$$

where, X is the state vector and u is the control vector. This can be expressed as;

$$\boldsymbol{X} = [\boldsymbol{i_{pv}}, \boldsymbol{V_{dcpv}}, \boldsymbol{i_{fdpv}}, \boldsymbol{i_{fqpv}}, \boldsymbol{i_{codpv}}, \boldsymbol{i_{coqpv}}, \boldsymbol{V_{cdpv}}, \boldsymbol{V_{cqpv}}, \boldsymbol{\theta_s}, \boldsymbol{\omega_t}, \boldsymbol{\delta_w}, \boldsymbol{\omega_w}, \boldsymbol{i_{pmsgdw}}, \boldsymbol{i_{pmsgqw}},$$

$$\boldsymbol{V_{dcw}}, \boldsymbol{i_{fdw}}, \boldsymbol{i_{fqw}}, \boldsymbol{i_{codw}}, \boldsymbol{i_{coqw}}, \boldsymbol{V_{cdw}}, \boldsymbol{V_{cqw}}, \boldsymbol{\delta_a}, \boldsymbol{\omega_a}, \boldsymbol{e_q'}, \boldsymbol{E_{fd}}, \boldsymbol{i_{dstat}}, \boldsymbol{i_{qstat}}, \boldsymbol{V_{dcstat}}]^{\boldsymbol{T}}$$

and,

$$\boldsymbol{u} = [\boldsymbol{m_{pv}}, \boldsymbol{\psi_{pv}}, \boldsymbol{m_{rw}}, \boldsymbol{m_{invw}}, \boldsymbol{\psi_{invw}}, \boldsymbol{m_{stat}}, \boldsymbol{\psi_{stat}}]^{\boldsymbol{T}}$$

4.2 Autonomous Mode of Operation

Applying KCL at the PCC; we get,

$$i_{copv} + i_{cow} + i_{ta} + i_{stat} = i_l \tag{4.18}$$

In terms of d-q axes; (4.18) becomes as;

$$i_{codpv} + i_{codw} + i_{tda} + i_{dstat} = i_{dl} \tag{4.19}$$

and,

$$i_{coqpv} + i_{coqw} + i_{tqa} + i_{qstat} = i_{ql} \tag{4.20}$$

Let us model the load at the PCC by an admittance $Y = g - jb$. The load current then can be expressed as;

$$i_l = V_{mg}Y$$

i.e. $i_l = V_{mg}(g - jb)$ (4.21)

In terms of d-q axes; (4.21) becomes as;

$$i_{dl} + ji_{ql} = (V_{dmg} + jV_{qmg})(g - jb)$$

i.e. $i_{dl} + ji_{ql} = gV_{dmg} - jbV_{dmg} + jgV_{qmg} + bV_{qmg}$

i.e. $i_{dl} + ji_{ql} = (gV_{dmg} + bV_{dmg}) + j(gV_{qmg} - bV_{dmg})$ (4.22)

Equating real and imaginary parts; we get,

$$i_{dl} = gV_{dmg} + bV_{dmg} \tag{4.23}$$

and,

$$i_{ql} = gV_{qmg} - bV_{dmg} \tag{4.24}$$

Substituting the values of i_{tda} and i_{dl} from (3.79) and (4.23) respectively into (4.19); we get,

$$i_{codpv} + i_{codw} + \frac{-R_{ta}V_{dmg} + (e_q{}' - V_{qmg})(x_{qa} + x_{ta})}{R_{ta}{}^2 + (x_{da}{}' + x_{ta})(x_{qa} + x_{ta})} + i_{dstat} = gV_{dmg} + bV_{dmg} \quad (4.25)$$

Let; $X_1 = x_{da}{}' + x_{ta}$

$X_2 = x_{qa} + x_{ta}$

$Z_1 = R_{ta}{}^2 + X_1X_2$

Using these variables in (4.25); we get,

$$i_{codpv} + i_{codw} + \frac{-R_{ta}V_{dmg} + (e_q{}' - V_{qmg})X_2}{Z_1} + i_{dstat} = gV_{dmg} + bV_{dmg}$$

i.e. $Z_1\left(i_{codpv} + i_{codw} + i_{dstat}\right) - R_{ta}V_{dmg} + X_2e_q{}' - X_2V_{qmg} = gZ_1V_{dmg} + bZ_1V_{qmg}$

i.e. $(gZ_1 + R_{ta})V_{dmg} + (bZ_1 + X_2)V_{qmg} = Z_1\left(i_{codpv} + i_{codw} + i_{dstat}\right) + X_2e_q{}' \quad (4.26)$

Similarly, substituting the values of i_{tqa} and i_{ql} from (3.80) and (4.24) respectively into (4.20); we get,

$$i_{coqpv} + i_{coqw} + \frac{V_{dmg}(x'_{da} + x_{ta})(x_{qa} + x_{ta}) + R_{ta}(e_q{}' - V_{qmg})(x_{qa} + x_{ta})}{(x_{qa} + x_{ta})[R_{ta}{}^2 + (x_{da}{}' + x_{ta})(x_{qa} + x_{ta})]} + i_{qstat} = gV_{qmg} - bV_{dmg}$$

(4.27)

In terms of X_1, X_2 and Z_1 as in the case of d-axes current; (4.27) becomes as;

$$i_{coqpv} + i_{coqw} + \frac{X_1X_2V_{dmg} + R_{ta}(e_q{}' - V_{qmg})X_2}{Z_1X_2} + i_{qstat} = gV_{qmg} - bV_{dmg}$$

i.e. $Z_1X_2\left(i_{coqpv} + i_{coqw} + i_{qstat}\right) + X_1X_2V_{dmg} + X_2R_{ta}e_q{}' - X_2R_{ta}V_{qmg} = gZ_1X_2V_{qmg} - bZ_1X_2V_{dmg}$

i.e. $(bZ_1X_2 + X_1X_2)V_{dmg} - X_2(gZ_1 + R_{ta})V_{qmg} = -Z_1X_2\left(i_{coqpv} + i_{coqw} + i_{qstat}\right) - X_2R_{ta}e_q{}' \quad (4.28)$

Let (4.26) and (4.28) be expressed as;

$$AV_{dmg} + BV_{qmg} = Z_1\left(i_{codpv} + i_{codw} + i_{dstat}\right) + X_2 e_q{}'$$

i.e. $V_{dmg} = \frac{1}{A}[Z_1\left(i_{codpv} + i_{codw} + i_{dstat}\right) + X_2 e_q{}' - BV_{qmg}]$ (4.29)

and,

$$CV_{dmg} - AX_2 V_{qmg} = -Z_1 X_2\left(i_{coqpv} + i_{coqw} + i_{qstat}\right) - X_2 R_{ta} e_q{}' \quad (4.30)$$

where,

$$A = gZ_1 + R_{ta}$$

$$B = bZ_1 + X_2$$

$$C = bZ_1 X_2 + X_1 X_2$$

Putting the values of V_{dmg} from (4.29) into (4.30); we get,

$$C \times \frac{1}{A}\left[Z_1\left(i_{codpv} + i_{codw} + i_{dstat}\right) + X_2 e_q{}' - BV_{qmg}\right] - AX_2 V_{qmg} = -Z_1 X_2\left(i_{coqpv} + i_{coqw} + i_{qstat}\right) - X_2 R_{ta} e_q{}'$$

i.e. $\frac{C}{A} Z_1\left(i_{codpv} + i_{codw} + i_{dstat}\right) + \frac{C}{A} X_2 e_q{}' - \frac{BC}{A} V_{qmg} - AX_2 V_{qmg} = -Z_1 X_2\left(i_{coqpv} + i_{coqw} + i_{qstat}\right) - X_2 R_{ta} e_q{}'$

i.e. $\frac{C}{A} Z_1\left(i_{codpv} + i_{codw} + i_{dstat}\right) + \left(\frac{C}{A} + R_{ta}\right) X_2 e_q{}' + Z_1 X_2\left(i_{coqpv} + i_{coqw} + i_{qstat}\right) - \left(\frac{BC}{A} + AX_2\right) V_{qmg} = 0$

i.e. $\left(\frac{BC + A^2 X_2}{A}\right) V_{qmg} = \frac{C}{A} Z_1\left(i_{codpv} + i_{codw} + i_{dstat}\right) + \left(\frac{C + AR_{ta}}{A}\right) X_2 e_q{}' + Z_1 X_2\left(i_{coqpv} + i_{coqw} + i_{qstat}\right)$

i.e. $V_{qmg} = \frac{1}{BC + A^2 X_2}[CZ_1\left(i_{codpv} + i_{codw} + i_{dstat}\right) + (C + AR_{ta}) X_2 e_q{}' + AZ_1 X_2\left(i_{coqpv} + i_{coqw} + i_{qstat}\right)]$

Let; $BC + A^2X_2 = Den$

So,$V_{qmg} = \frac{1}{Den} CZ_1\left(i_{codpv} + i_{codw} + i_{dstat}\right) + \frac{1}{Den}(C + AR_{ta})X_2 e_q{}' + \frac{1}{Den} AZ_1X_2\left(i_{coqpv} + i_{coqw} + i_{qstat}\right)$

i.e. $V_{qmg} = D\left(i_{codpv} + i_{codw} + i_{dstat}\right) + Ee_q{}' + F\left(i_{coqpv} + i_{coqw} + i_{qstat}\right)$ (4.31)

where,

$$D = \frac{1}{Den} CZ_1$$

$$E = \frac{1}{Den}(C + AR_{ta})X_2$$

$$F = \frac{1}{Den} AZ_1X_2$$

Using these values; V_{dmg} and V_{qmg} can be determined while operating in autonomous mode; and then can be used in the state equations of different component models. Thus, the state equation takes the form of;

$$\dot{X} = f(X, u)$$

where, X is the state vector and u is the control vector. This can be expressed as;

$$\boldsymbol{X} = [\boldsymbol{i_{pv}}, \boldsymbol{V_{dcpv}}, \boldsymbol{i_{fdpv}}, \boldsymbol{i_{fqpv}}, \boldsymbol{i_{codpv}}, \boldsymbol{i_{coqpv}}, \boldsymbol{V_{cdpv}}, \boldsymbol{V_{cqpv}}, \boldsymbol{\theta_s}, \boldsymbol{\omega_t}, \boldsymbol{\delta_w}, \boldsymbol{\omega_w}, \boldsymbol{i_{pmsgdw}}, \boldsymbol{i_{pmsgqw}},$$

$$\boldsymbol{V_{dcw}}, \boldsymbol{i_{fdw}}, \boldsymbol{i_{fqw}}, \boldsymbol{i_{codw}}, \boldsymbol{i_{coqw}}, \boldsymbol{V_{cdw}}, \boldsymbol{V_{cqw}}, \boldsymbol{\delta_a}, \boldsymbol{\omega_a}, \boldsymbol{e_q{}'}, \boldsymbol{E_{fd}}, \boldsymbol{i_{dstat}}, \boldsymbol{i_{qstat}}, \boldsymbol{V_{dcstat}}]^{\boldsymbol{T}}$$

and,

$$\boldsymbol{u} = [\boldsymbol{m_{pv}}, \boldsymbol{\psi_{pv}}, \boldsymbol{m_{rw}}, \boldsymbol{m_{invw}}, \boldsymbol{\psi_{invw}}, \boldsymbol{m_{stat}}, \boldsymbol{\psi_{stat}}]^{\boldsymbol{T}}$$

Chapter 5

Simulation Results and Analysis

In this chapter, the dynamically modeled microgrid system with photovoltaic (PV), wind energy conversion system (WECS), microalternator and static synchronous compensator (STATCOM) operating in both non-autonomous and autonomous modes has been considered for heuristically analyzing the system performance. Initial values for running the system at the steady state has been calculated by using the general law of power systems. This is then used in the MATLAB ode program for running the system in both non-autonomous and autonomous modes. In this study, at first the observed system is allowed to run in non-autonomous mode; and has been switched to autonomous mode after encountering permanent fault in the main grid. Temporary disturbance has been given and the system performance has been observed. The system performance has also been observed when permanent fault is encountered. It is expected that during temporary disturbances, the system must continue to operate in non-autonomous mode but during permanent fault it is to be shifted to the autonomous mode by opening the circuit braker and isolator between the microgrid and the main grid.

For both the cases, here in this section, various system performances such as microgrid voltage, total active and reactive power of microgrid, PV array current, PV DC-link voltage, net output PV current, PMSG current, WECS DC-link voltage, net output WECS current, synchronous generator field voltage along d-axis, internal voltage along q-axis, microalternator rotor speed, STATCOM DC-link voltage, reactive power supplied by STATCOM and STATCOM current has been observed and heuristically analyzed.

5.1 Overall Microgrid Response

Fig. 5.1, 5.2 and 5.3 shows the plots for voltage, total active power and total reactive power of the microgrid or point of common coupling (PCC) respectively for the microgrid system

operating in non-autonomous and autonomous modes. Here, temporary disturbances in the main grid is simulated from 1 sec to 1.1 sec; which the system itself clears out by the use of the controller and make it to return back to the steady state. But when a permanent fault for 0.5 sec is simulated from 8.4 sec to 8.9 sec, the system could not return back to the steady state and kept on oscillating. Hence, the system is switched to an autonomous mode. Then, within 0.5 sec to 1 sec, the system is found to deliver power to local loads efficiently by operating in an autonomous mode. Here, at steady state, before and after the fault; the microgrid voltage, active power and reactive power has been found to be maintained constant at about 1 p.u, 1.3 p.u and 0.02 p.u respectively.

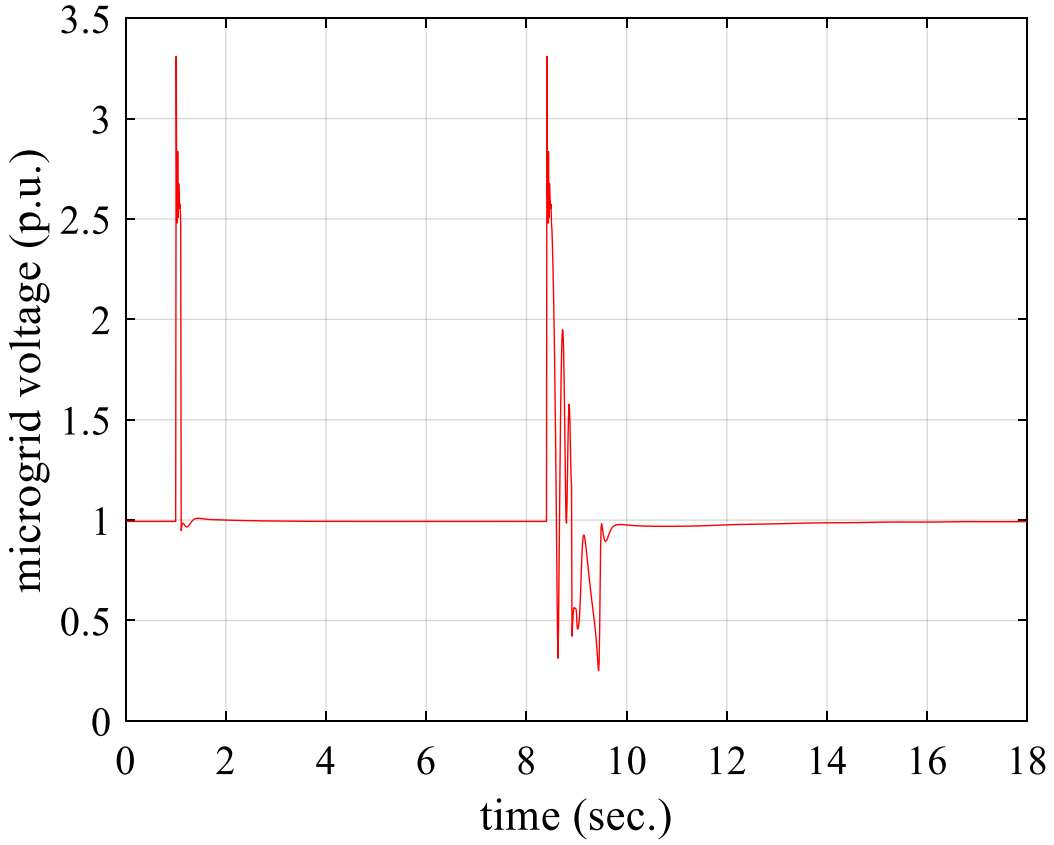

Fig. 5. 1 Microgrid voltage vs time

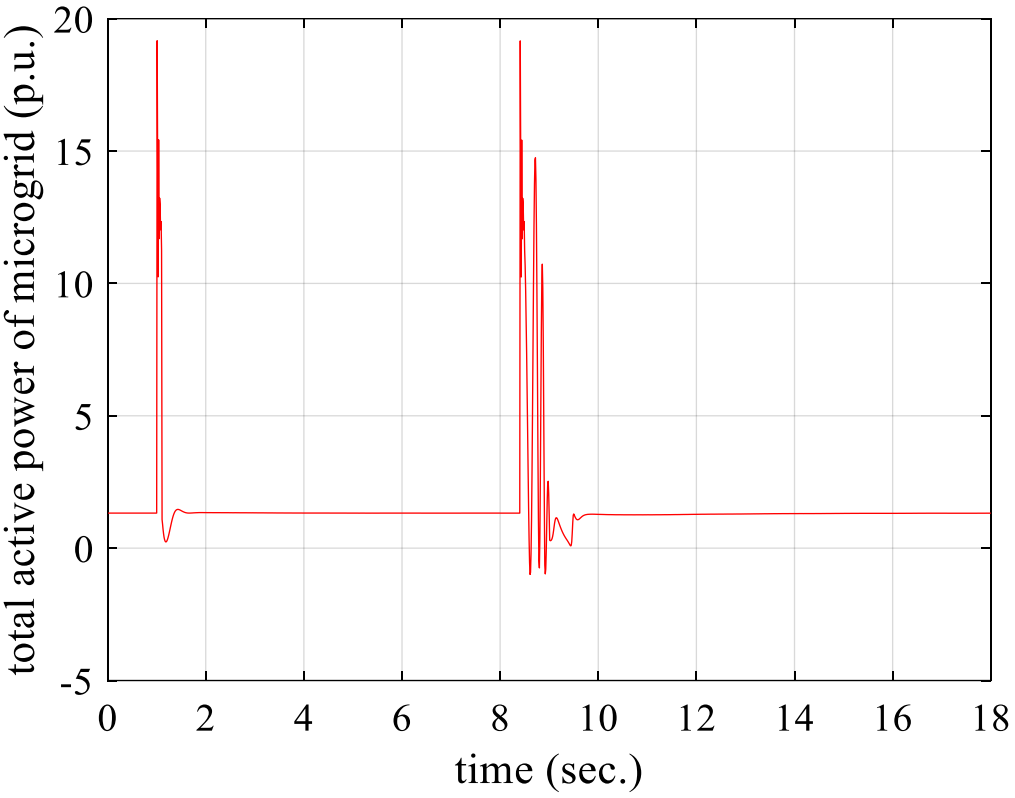

Fig. 5. 2 Total active power of microgrid vs time

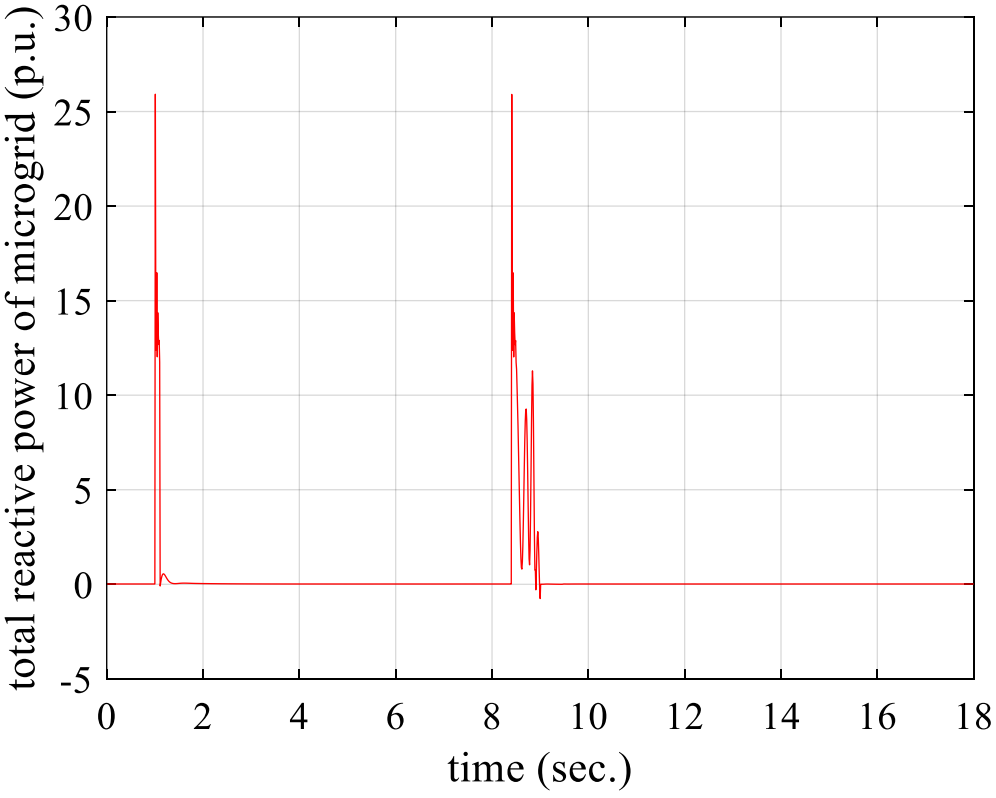

Fig. 5. 3 Total reactive power of microgrid vs time

5.2 PV System Response

Fig. 5.4, 5.5 and 5.6 shows the plots for PV array current, PV DC-link voltage and net output PV current respectively for the microgrid system operating in non-autonomous and autonomous modes. Here, during the temporary disturbances, the PV array current varies from 0.65 p.u to 0.7 p.u and PV DC-link voltage varies from 0.99 p.u to 1.06 p.u. But the net output PV current shortly spikes due to the distortion in transmission to the main grid. As controller is used in the network, this increased current settles down to some steady state value quickly. But for example, if permanent fault for 0.5 sec from 8.4 sec to 8.9 sec is encountered in the main grid, the system could not return back to the steady state and kept on oscillating. Then, once the system is switched to an autonomous mode; within 2 to 3 sec, the system is found to deliver power to local loads efficiently. Here, at steady state, before and after the fault; the PV array current, PV DC-link voltage and net output PV current has been found to be maintained constant at about 0.696 p.u, 1 p.u and 0.57 p.u respectively.

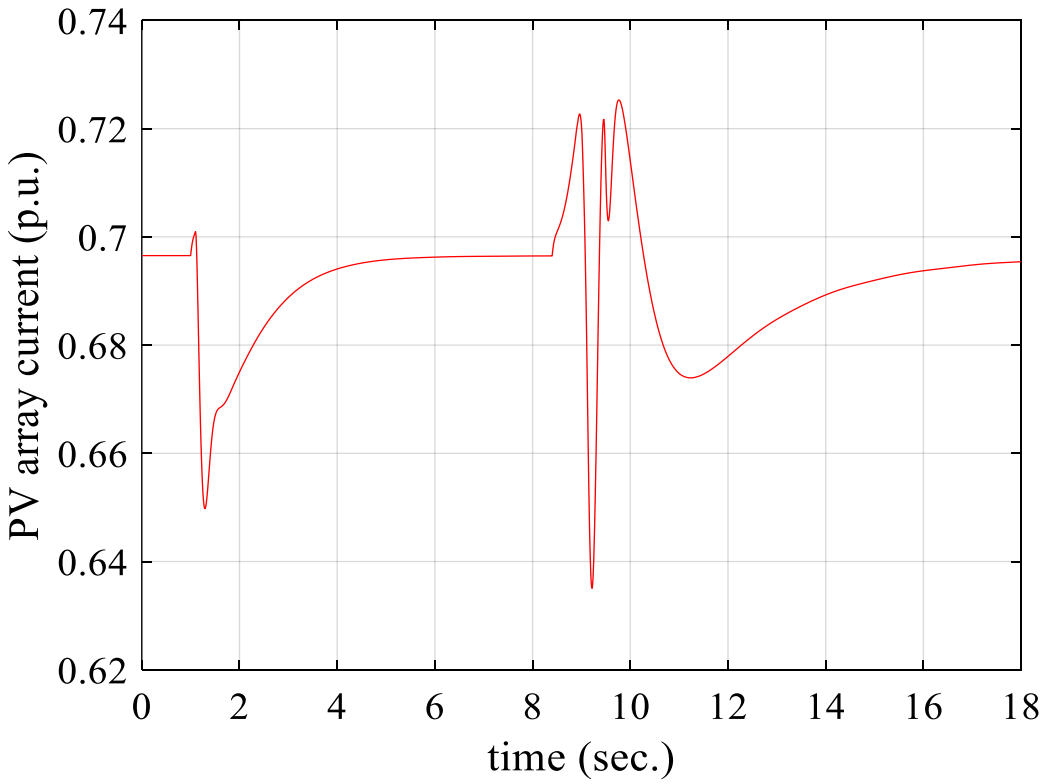

Fig. 5. 4 PV array current vs time

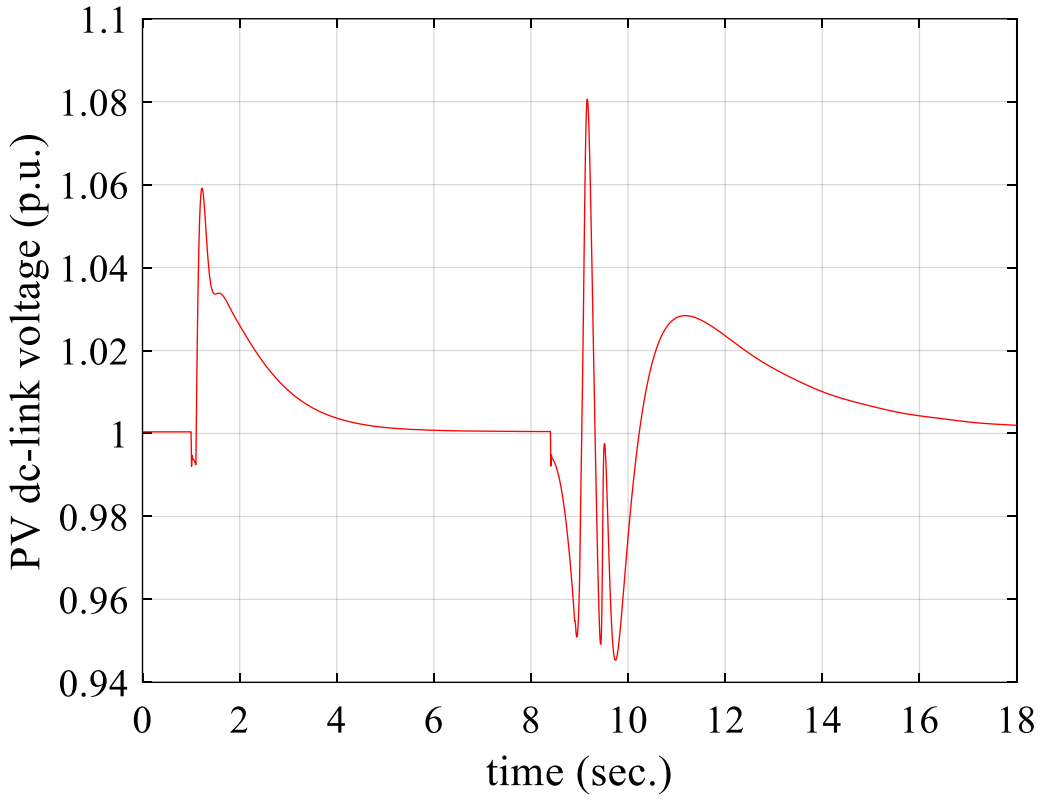

Fig. 5. 5 PV DC-link voltage vs time

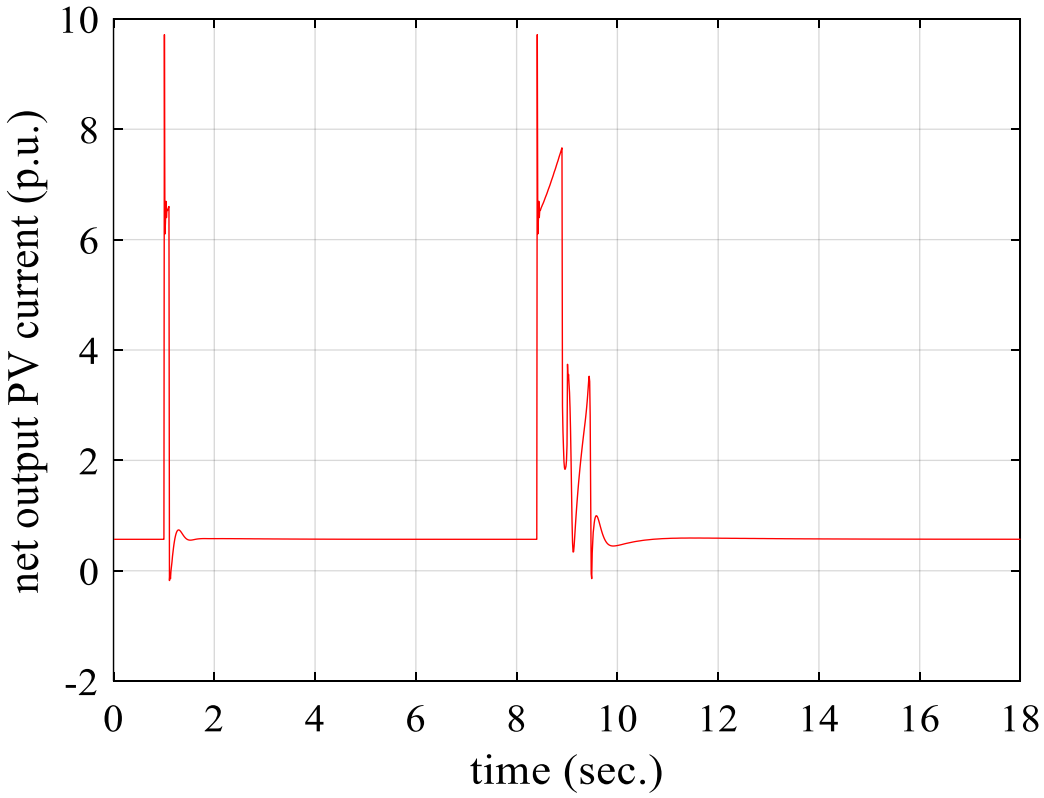

Fig. 5. 6 Net output PV current vs time

5.3 WECS Response

Figure 5.7, 5.8 and 5.9 shows the plots for PMSG current, WECS DC-link voltage and net output WECS current respectively for the microgrid system operating in non-autonomous and autonomous modes. Here, during the temporary disturbances, the PMSG current varies from 0.53 p.u to 0.62 p.u and WECS DC-link voltage varies from 0.99 p.u to 1.06 p.u. But the net output WECS current shortly spikes due to time lag in controller action; and settles down to some steady state value quickly. Similar to case of PV system, if permanent fault for 0.5 sec from 8.4 sec to 8.9 sec is encountered in the main grid, the system could not return back to the steady state and kept on oscillating. Then, once the system is switched to an autonomous mode; within few seconds, the WECS is also found of contributing power to the local loads. Here, at steady state, before and after the fault; the PMSG current, WECS DC-link voltage and net output WECS current has been found to be maintained constant at about 0.6 p.u, 1 p.u and 0.57 p.u respectively.

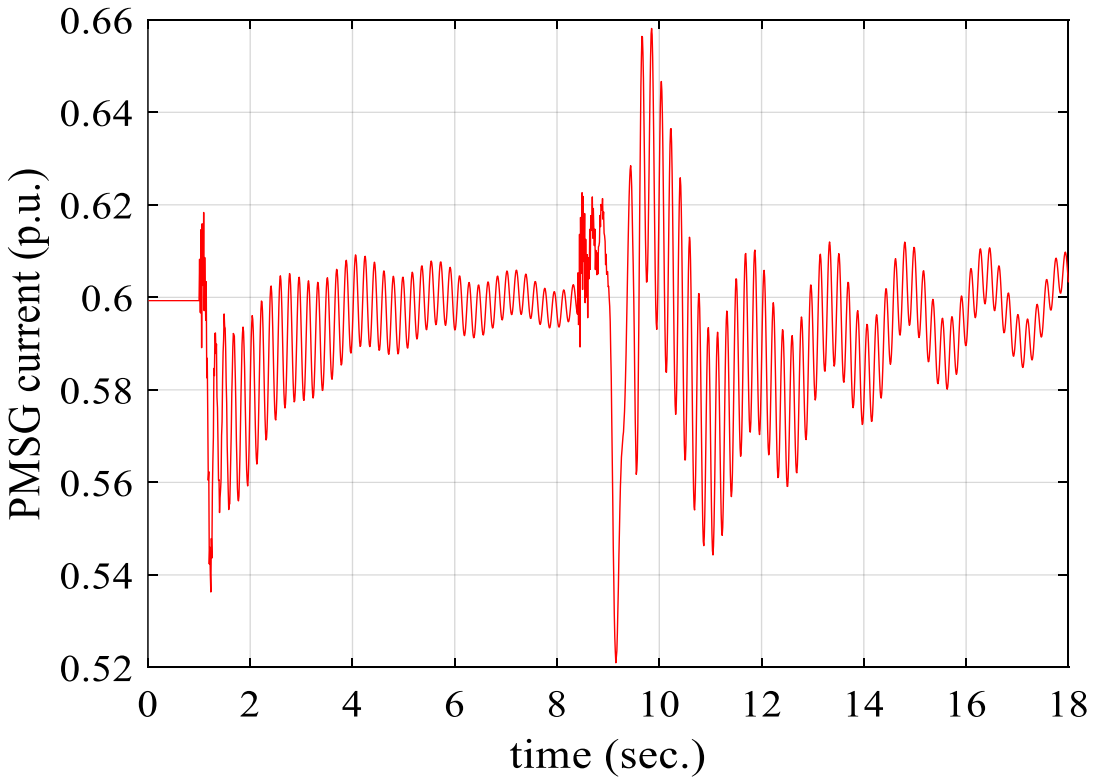

Fig. 5. 7 PMSG current vs time

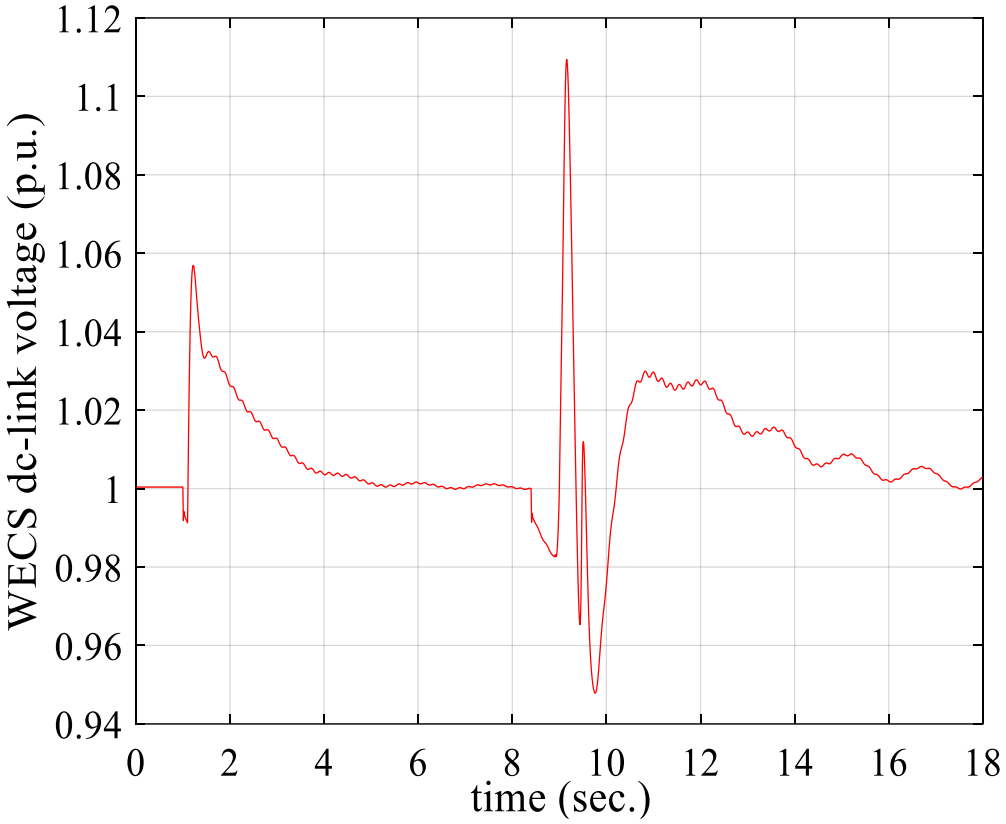

Fig. 5. 8 WECS DC-link voltage vs time

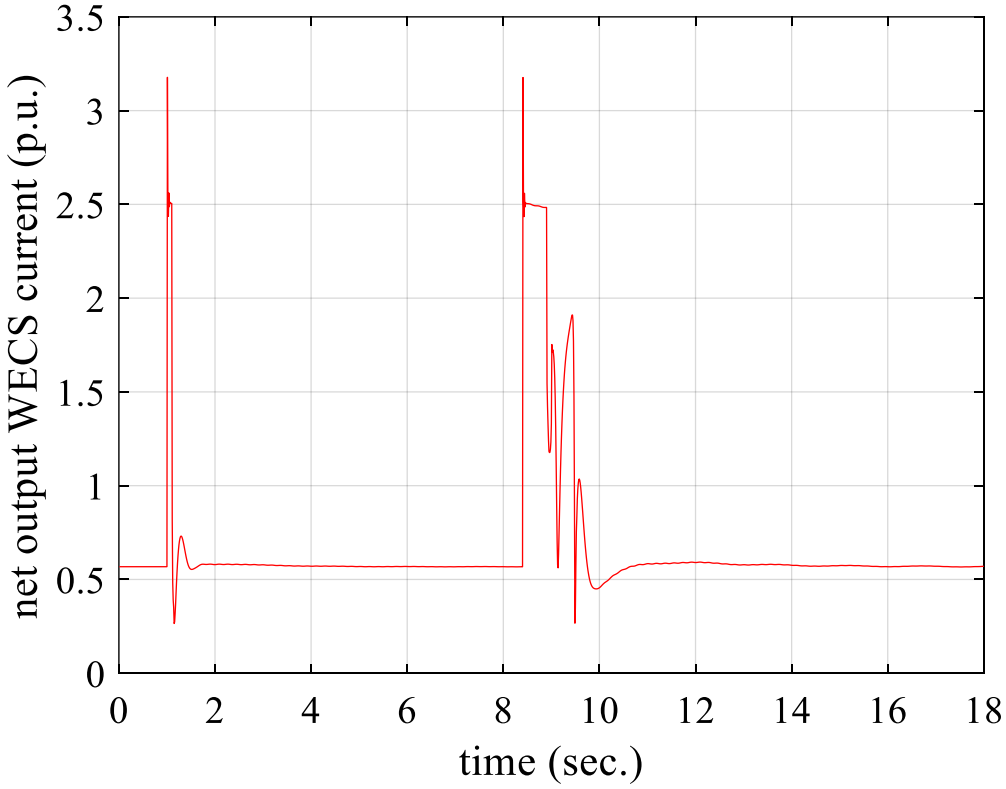

Fig. 5. 9 Net output WECS current vs time

5.4 Microalternator System Response

Fig. 5.10, 5.11 and 5.12 shows the plots for synchronous generator field voltage along d-axis, internal voltage along q-axis and microlaternator rotor speed respectively for the microgrid system operating in non-autonomous and autonomous modes. Just like in PV system and WECS, during temporary disturbances, the voltages and rotor speed of microalternator system oscillates for few seconds and gets back to the steady state by its physical inertia. Here, rotor speed varies between 0.98 p.u to 1.01 p.u. But once a permanent fault is encountered, the system cannot get enough inertia by itself to bring the whole power system network into steady state. Then, once the system is switched to an autonomous mode; within few seconds, the microalternator system is also found of contributing power to the local loads. Here, at steady state, synchronous generator field voltage along d-axis, internal voltage along q-axis and microlaternator rotor speed has been found to be maintained constant at about 1.18 p.u, 1.06 p.u and 1 p.u respectively.

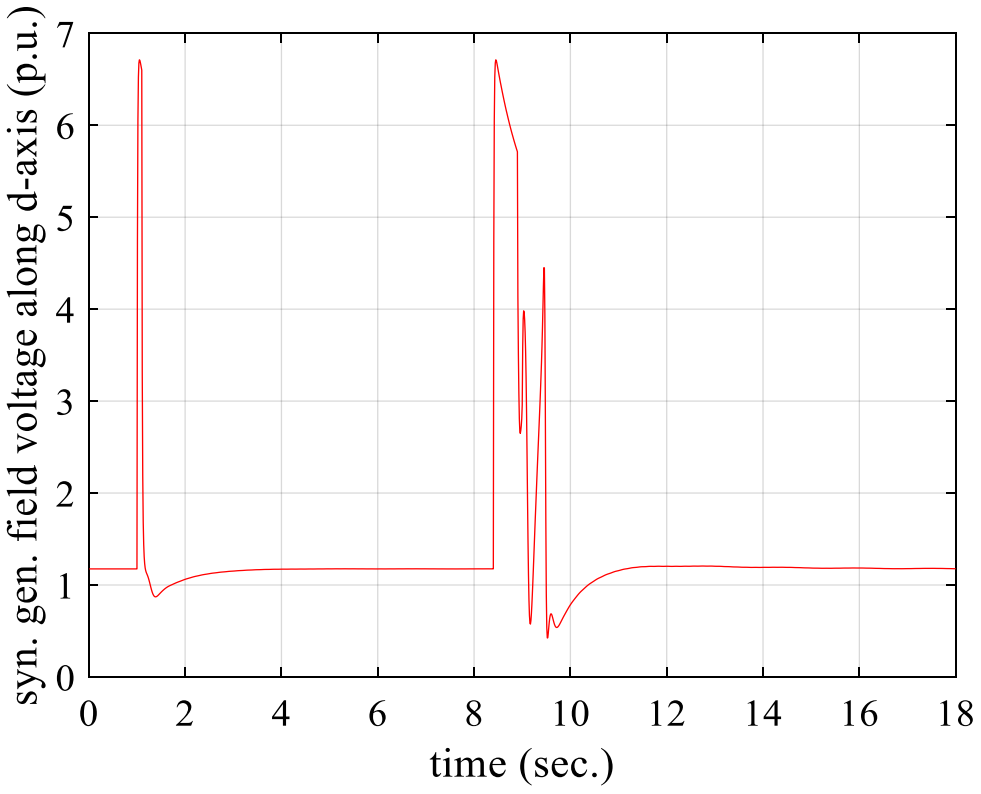

Fig. 5. 10 Synchronous generator field voltage along d-axis vs time

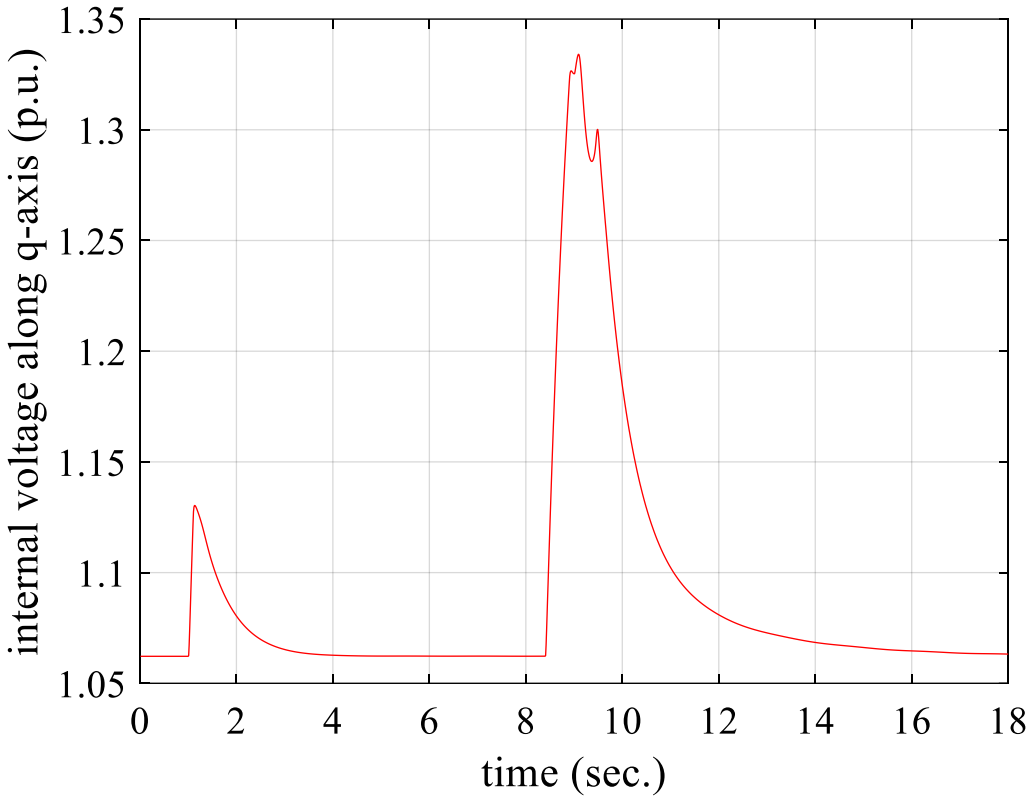

Fig. 5. 11 Internal voltage along q-axis vs time

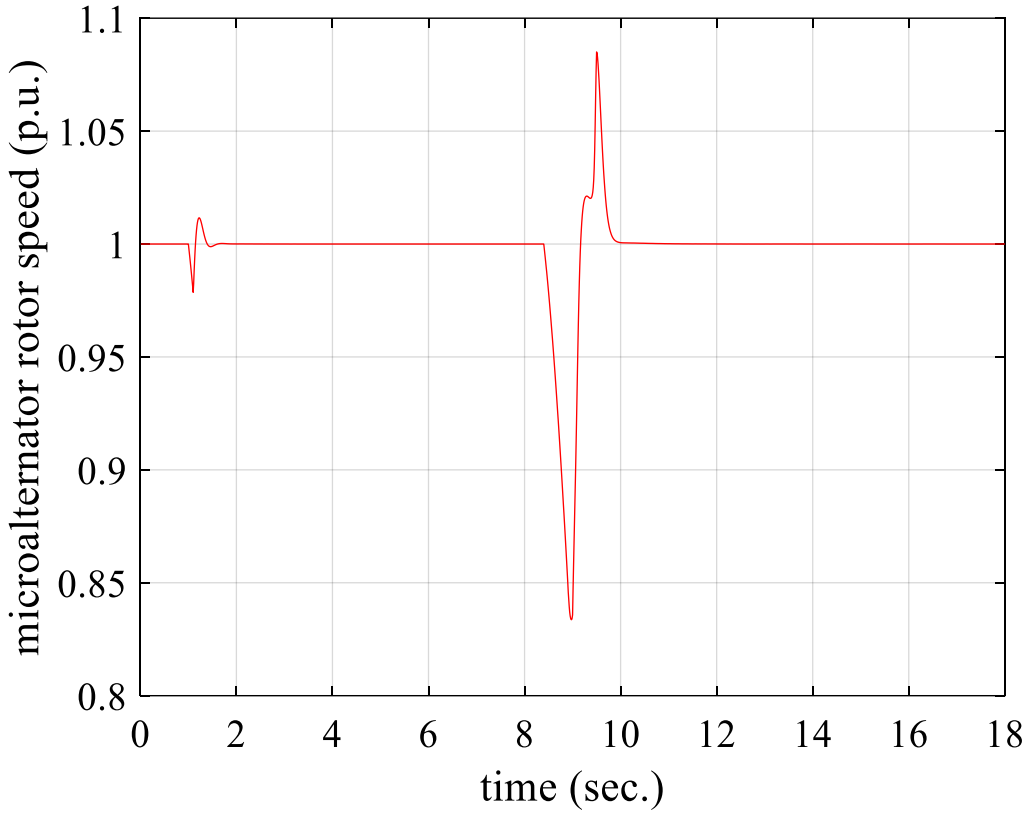

Fig. 5. 12 Microalternator rotor speed vs time

5.5 STATCOM Response

Fig. 5.13, 5.14 and 5.15 shows the plots for STATCOM DC-link voltage, reactive power supplied by the STATCOM and STATCOM current respectively for the microgrid system operating in non-autonomous and autonomous modes. As STATCOM acts as a central supervisory controller, it supplies reactive power during contingencies in the grid. Here, during both temporary and permanent disturbances; though the STATCOM DC-link voltage decreases, the STATCOM reactive power and current increases to support the microgrid voltage. From the plots, it can also be observed that during steady state, the STATCOM DC-link voltage remains constant at about 0.97 p.u. But at the same time, the STATCOM reactive power and STATCOM current has been found to be zero as STATCOM normally do not play any major role in normal operating state.

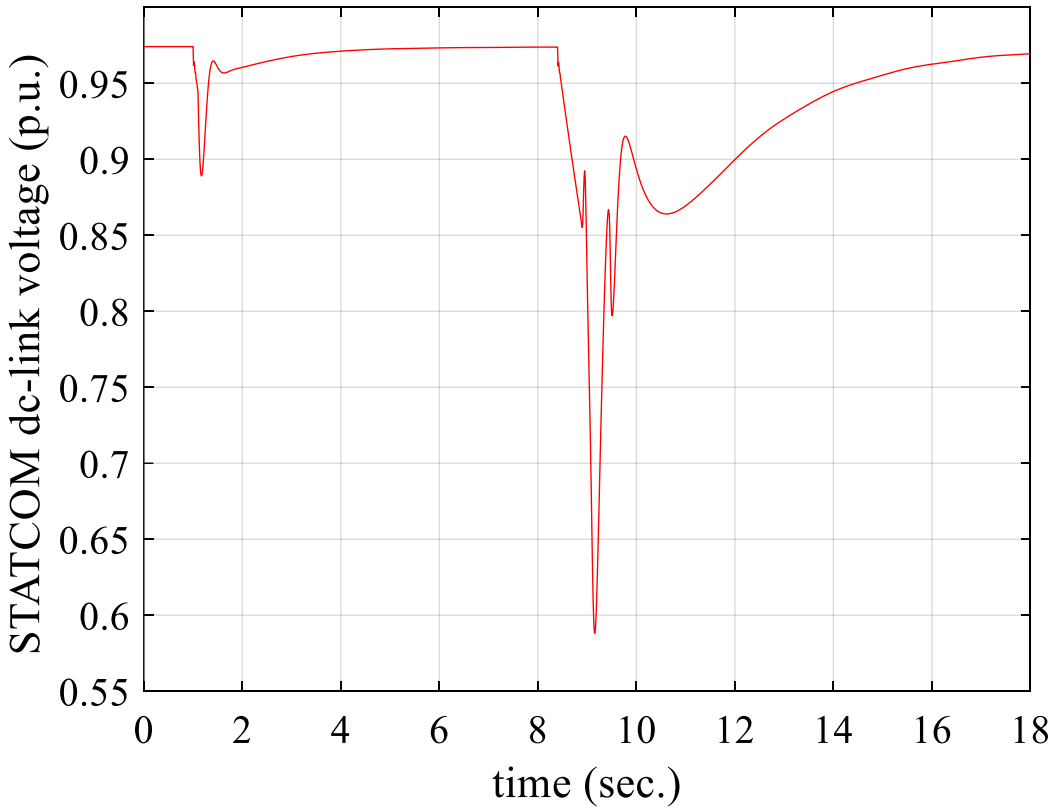

Fig. 5. 13 STATCOM DC-link voltage vs time

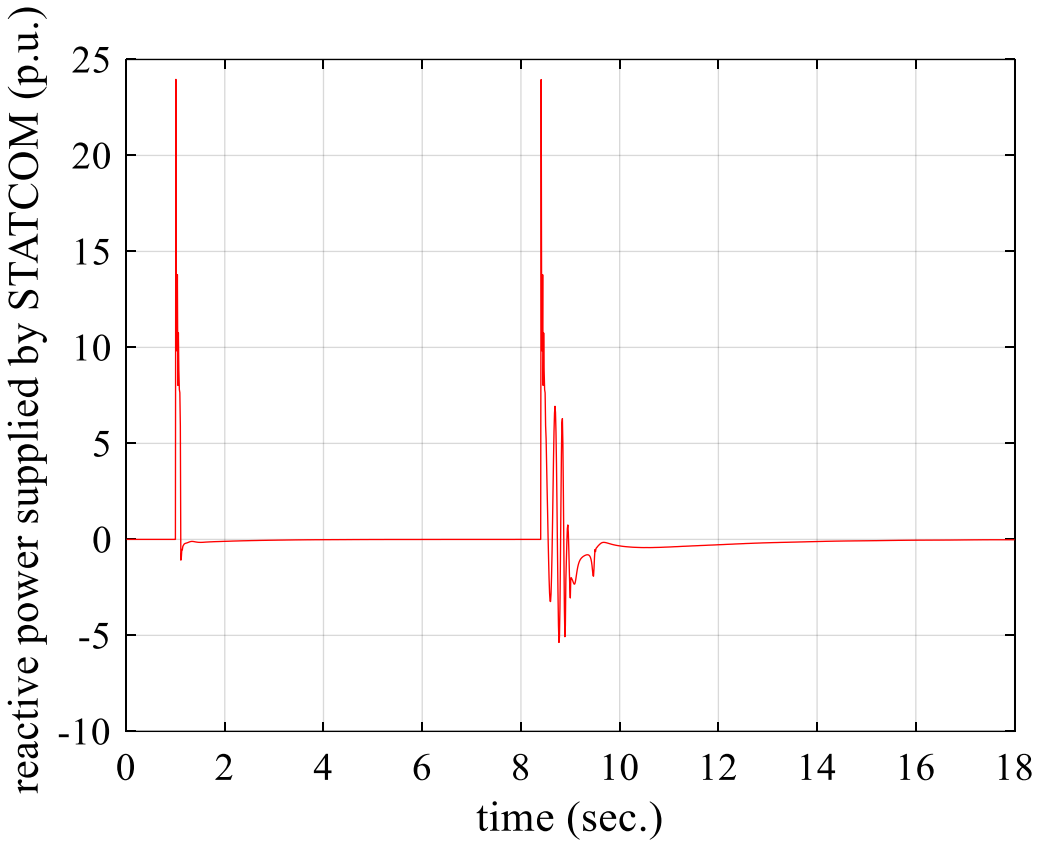

Fig. 5. 14 Reactive power supplied by STATCOM vs time

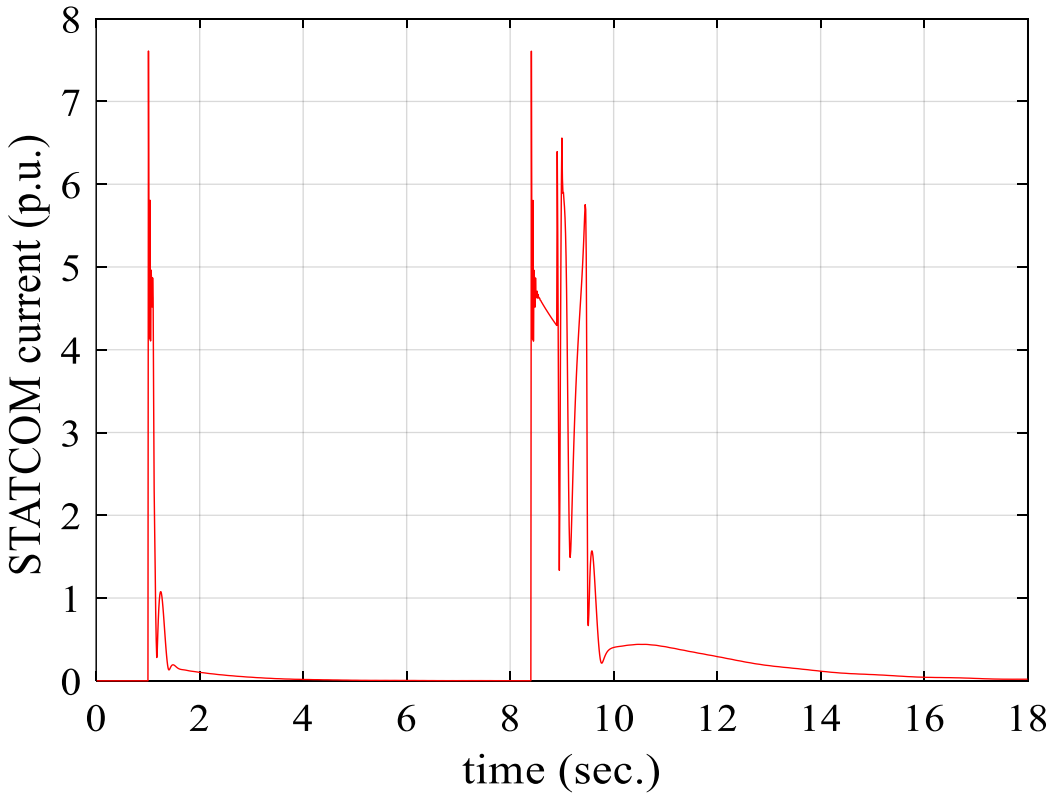

Fig. 5. 15 STATCOM current vs time

From the plots for different mcirogrid components, it is observed that the system can efficiently run in both non-autonomous and autonomous modes depending on the level of disturbances. Here, in this dynamically modeled microgrid system, when disturbance or fault is encountered for upto 0.2 sec (here, 0.19 sec) between the main grid and the microgrid, it is seen that the system can settle down itself to return back to the steady state. But when the disturbance is not cleared within few cycles; then in such a case, the system is found to be shifted to the autonomous mode. The mode transition is performed by the set of circuit breaker and isolator placed between the microgrid and the main grid. Though spikes are encountered during the transition, it is seen that they are slowly settled down to the steady state value. The quick settlement of the fluctuating waveform is because of the use of STATCOM with capacitor energy storage based central controller.

Chapter 6

Conclusion and Future Work

6.1 Summary

The dynamic modeling and performance analysis of a microgrid system with photovoltaic (PV), wind energy conversion system (WECS), microalternator and static synchronous compensator (STATCOM) has been performed in this project. The inertial type of DG; i.e. microalternator has been directly coupled to the microgrid while the non-inertial type of DGs; i.e. PV and WECS has been connected to the microgrid via power conditioning unit and filter circuitry. The STATCOM here is connected to the microgrid via capacitor energy storage device.

Non-linear state equations for all the components in use has been dynamically modeled; and they were combined together to form a complete system capable of operating in both autonomous and non-autonomous modes. 28 different state equations from different system components; i.e. PV, WECS, microalternator and STATCOM has been used here for modeling the microgrid system. The system has been modeled by using MATLAB ode program; and has been solved by ‘ode 45’ solver.

Different types of disturbances; i.e. temporary and permanent disturbances has been simulated to heuristically analyze the system performances. The resiliency to continue in the same operating mode; and the successful transition between the modes during abnormal condition has been analyzed. The role of STATCOM in maintaining microgrid voltage during contingencies has also been analyzed in this project.

Finally, it is ensured that the load connected to the microgrid could always get power of desired voltage and frequency irrespective of duration of contingencies and mode of operation.

6.2 Conclusion

From non-linear analysis, it was observed that the designed system can operate in both autonomous and non-autonomous modes depending on the need of the system. When the system itself can run at steady state after the disturbances, the system continues to run in non-autonomous mode. But, if the inertia of the system could not bring the whole system back to a steady state; then in such a case, it detaches itself from the main grid to run in an autonomous mode.

It was also observed that the properly modeled STATCOM with capacitor energy storage system can support the grid voltage and frequency during contingencies. In this project, they were used for supplying active and reactive power to the microgrid during contingencies. It thus assists on maintaining the microgrid voltage level and frequency.

In overall, the dynamically modeled microgrid system has been observed and found that the designed system model is well-efficient to operate in both autonomous and non-autonomous modes. The simulation result also shows that the transition of operating modes is smooth and does not create fluctuation in output power for a longer time.

6.3 Future Work

The work that can be carried out in this area are illustrated as:

- The hybrid microgrid consisting of both AC and DC networks linked together can be designed by using multi-bidirectional converters.
- Different energy storage devices such as supercapacitors, superconducting magnetic energy storage (SMES) devices can be used for regulating the active power flow in the microgrid.

- Different FACTS devices other than STATCOM can be used for regulating the reactive power flow during the transients.
- Various control and optimization techniques can be implemented for controlling the overall power system network.

References

[1] L. Al-Ghussain, "Global warming: review on driving forces and mitigation", *Environmental Progress & Sustainable Energy*, vol. 38, no. 1, pp. 13-21, 2018.

[2] J. Carrasco et al., "Power-Electronic Systems for the Grid Integration of Renewable Energy Sources: A Survey", *IEEE Transactions on Industrial Electronics*, vol. 53, no. 4, pp. 1002-1016, 2006.

[3] E. Howland, "Microgrid Costs and How to Lower Them: Microgrid 2021", *Microgrid Knowledge*, 2022. [Online].

[4] M. El-Moursi and A. Sharaf, "Novel reactive power controllers for the STATCOM and SSSC", *Electric Power Systems Research*, vol. 76, no. 4, pp. 228-241, 2006.

[5] R. Madurai Elavarasan, A. Ghosh, T. K. Mallick, A. Krishnamurthy and M. Saravanan, "Investigations on Performance Enhancement Measures of the Bidirectional Converter in PV–Wind Interconnected Microgrid System", *Energies*, vol. 12, no. 14, p. 2672, 2019.

[6] F. Hasan, P. Nabanita, S. Islam and T. Haidar, "Developing a Voltage Control Methodology for Renewable Integrated Microgrid", *2019 International Conference on Energy and Power Engineering (ICEPE)*, 2019.

[7] S. D'silva, M. Shadmand, S. Bayhan and H. Abu-Rub, "Towards Grid of Microgrids: Seamless Transition between Grid-Connected and Islanded Modes of Operation", *IEEE Open Journal of the Industrial Electronics Society*, vol. 1, pp. 66-81, 2020.

[8] B. Satish and S. Bhuvaneswari, "Control of microgrid — A review", *2014 International Conference on Advances in Green Energy (ICAGE)*, 2014.

[9] B. Jena and A. Choudhury, "Voltage and frequency stabilisation in a micro-hydro-PV based hybrid microgrid using FLC based STATCOM equipped with BESS", *2017 International Conference on Circuit ,Power and Computing Technologies (ICCPCT)*, 2017.

[10] G. Talapur, H. Suryawanshi, L. Xu and A. Shitole, "A Reliable Microgrid With Seamless Transition Between Grid Connected and Islanded Mode for Residential Community With Enhanced Power Quality", *IEEE Transactions on Industry Applications*, vol. 54, no. 5, pp. 5246-5255, 2018.

[11] N. Ghanbari, S. Bhattacharya and M. Mobarrez, "Modeling and Stability Analysis of a DC Microgrid Employing Distributed Control Algorithm", *2018 9th IEEE International Symposium on Power Electronics for Distributed Generation Systems (PEDG)*, 2018.

[12] D. Sahidin, T. Desmana Rachmildha and D. Hamdani, "Power Quality Analysis of Solar PV/Micro-Hydro/Wind Renewable Energy Systems for Isolated Area", *2021 3rd International Conference on High Voltage Engineering and Power Systems (ICHVEPS)*, 2021.

[13] M. Gayatri, A. Parimi and A. Pavan Kumar, "A review of reactive power compensation techniques in microgrids", *Renewable and Sustainable Energy Reviews*, vol. 81, pp. 1030-1036, 2018.

[14] R. Sabzehgar, "Overview of Technical Challenges, Available Technologies and Ongoing Developments of AC/DC Microgrids", *Mendeley*, 2022. [Online].

[15] Y. Huo, S. Barcellona, G. Gruosso and L. Piegari, "Definition and Analysis of an Innovative Ancillary Service for Microgrid Stability Improvement", *2018 International Symposium on Power Electronics, Electrical Drives, Automation and Motion (SPEEDAM)*, 2018.

[16] L. Meegahapola, A. Sguarezi, J. Bryant, M. Gu, E. Conde D. and R. Cunha, "Power System Stability with Power-Electronic Converter Interfaced Renewable Power Generation: Present Issues and Future Trends", *Energies*, vol. 13, no. 13, p. 3441, 2020.

[17] K. Yap, C. Sarimuthu and J. Lim, "Virtual Inertia-Based Inverters for Mitigating Frequency Instability in Grid-Connected Renewable Energy System: A Review", *Applied Sciences*, vol. 9, no. 24, p. 5300, 2019.

[18] Y. Tan, D. Kirschen and N. Jenkins, "A Model of PV Generation Suitable for Stability Analysis", *IEEE Transactions on Energy Conversion*, vol. 19, no. 4, pp. 748-755, 2004.

[19] S. D'silva, M. Shadmand, S. Bayhan and H. Abu-Rub, "Towards Grid of Microgrids: Seamless Transition between Grid-Connected and Islanded Modes of Operation", *IEEE Open Journal of the Industrial Electronics Society*, vol. 1, pp. 66-81, 2020.

[20] W. Deng, X. Tang and Z. Qi, "Research on dynamic stability of hybrid wind/PV system based on Micro-Grid", *2008 International Conference on Electrical Machines and Systems*, pp. 2627-2632, 2008.

[21] A. S. Sedra and K. C. Smith, "Microelectronic Circuits". *London, U.K.: Oxford Univ. Press*, 2006.

[22] H. J. Moller, "Semiconductors for Solar Cells". *Norwood, MA: Artech House*, 1993.

[23] A.L. Fahrenbruch and R. H. Bube, "Fundamentals of solar cells: photovoltaic solar energy conversion", *Elsevier,* 2012.

[24] F. Lasnier and T.G. Ang, "Photovoltaic engineering handbook", *Routledge,* 2017.

[25] D. King, J. Kratochvil and W. Boyson, "Photovoltaic Array Performance Model", 2004.

[26] B. P. Sx, "Bp sx 150", pp. 1–4, 2001.

[27] R. Yan and T. K. Saha, "Development of simplified models for a single phase grid connected photovoltaic system", pp. 1-6, 2011.

[28] M. E. Ropp and S. Gonzalez, "Development of a MATLAB/simulink model of a single-phase grid-connected photovoltaic system", *Energy Conversion, IEEE Transactions on,* vol. 24, pp. 195-202, 2009.

[29] A. Canova, et al., "Electrical impact of photovoltaic plant in distributed network", *Industry Applications, IEEE Transactions on,* vol. 45, pp. 341-347, 2009.

[30] E. Liu, et al., "Distribution system voltage performance analysis for high-penetration photovoltaics", *National Renewable Energy Laboratory,* 2008.

[31] S. Achilles, et al., "Transmission system performance analysis for high-penetration photovoltaics", *National Renewable Energy Laboratory,* 2008.

[32] W. Qiao and D. Lu, "A Survey on Wind Turbine Condition Monitoring and Fault Diagnosis−Part I: Components and Subsystems", *IEEE Trans Ind. Electron,* vol. 62, no. 10, pp. 6536 – 6545, 2015.

[33] H. Polinder, F. van der Pijl, G.-J. de Vilder and P. Tavner, "Comparison of direct-drive and geared generator concepts for wind turbines", *IEEE Trans. Energy Convers*., vol. 21, no. 3, pp. 725–733, 2006.

[34] H. Geng and D. Xu, "Stability Analysis and Improvements for Variable-Speed Multipole Permanent Magnet Synchronous Generator-Based Wind Energy Conversion System", *IEEE Trans. On Sustainable Energy,* vol. 2, no. 4, pp. 459-467, 2011.

[35] F.A. Farret and M.G. Simões, "Integration of Alternative Sources of Energy", *Wiley IEEE Press,* 2006.

[36] F. Blaabjerg, M. Liserre and K. Ma, "Power Electronics Converters for Wind Turbine Systems," *IEEE Transactions on Industry Applications,* vol. 48, no. 2, pp. 708-719, 2012.

[37] R. Tiwari and N.R. Babu, "Recent developments of control strategies for wind energy conversion system", *Renewable and Sustainable Energy Reviews,* vol. 66, pp. 268-285, 2016.

[38] "Micro Alternator - Home Improvement - AliExpress", *Aliexpress.com*, 2022. [Online].

[39] Y.N.Yu, "Electric power system dynamics", *ACADEMIC PRESS, INC., 111 FIFTH AVE., NEW YORK, NY 10003, USA,* 1983.

[40] Y. Ma, A. Huang and X. Zhou, "A review of STATCOM on the electric power system", *2015 IEEE International Conference on Mechatronics and Automation (ICMA)*, 2015.

[41] Y. Chen, B. Mwinyiwiwa, Z. Wolanski and B. Ooi, "Regulating and equalizing DC capacitance voltages in multilevel STATCOM", *IEEE Transactions on Power Delivery*, vol. 12, no. 2, pp. 901-907, 1997.

[42] Y. Xu and F. Li, "Adaptive PI Control of STATCOM for Voltage Regulation", *IEEE Transactions on Power Delivery*, vol. 29, no. 3, pp. 1002-1011, 2014.

[43] Y. Chen and B. Ooi, "STATCOM based on multimodules of multilevel converters under multiple regulation feedback control", *IEEE Transactions on Power Electronics*, vol. 14, no. 5, pp. 959-965, 1999.

[44] M. Bhesaniya and A. Shukla, "Current Source Modular Multilevel Converter: Detailed Analysis and STATCOM Application", *IEEE Transactions on Power Delivery*, vol. 31, no. 1, pp. 323-333, 2016.

[45] Y. Ma, L. Cao, X. Zhou and Z. Gao, "The discussion on static synchronous compensator technology", *2016 IEEE International Conference on Mechatronics and Automation*, 2016.

[46] S. Muchande, S. Thale and R. Wandhare, "Integrated Solar PV-Battery and Micro-Hydro Based Low-Voltage Autonomous DC Microgrid for Rural Electrification", *2020 47th IEEE Photovoltaic Specialists Conference (PVSC)*, 2020.

[47] C. Smallwood, "Distributed generation in autonomous and non-autonomous micro grids", *2002 Rural Electric Power Conference. Papers Presented at the 46th Annual Conference (Cat. No. 02CH37360)*, 2002.

[48] R. Roofegari Nejad and S. Moghaddas Tafreshi, "Operation Planning of a Smart Microgrid Including Controllable Loads and Intermittent Energy Resources by

Considering Uncertainties", *Arabian Journal for Science and Engineering*, vol. 39, no. 8, pp. 6297-6315, 2014.

[49] S. Zhou, Y. Gu, W. Song, C. Wang, F. Bai and Y. Cai, "Research on Control Strategy of Grid-Connected Inverter in Microgrid System", *2019 IEEE 3rd Conference on Energy Internet and Energy System Integration (EI2)*, 2019.

[50] R. Zhao, Q. Li, H. Xu, Y. Wang and J. Guerrero, "Harmonic Current Suppression Strategy for Grid-Connected PWM Converters With LCL Filters", *IEEE Access*, vol. 7, pp. 16264-16273, 2019.

[51] J. R. Martí, "The AC Electrical Grid: Transitions into the Twenty-First Century", *Energy Transitions in History, RCC Perspectives*, no. 2, pp. 75–82, 2013.

[52] L. de Araujo, M. Villalva and T. Siqueira, "Autonomous microgrid with energy storage system", *2017 IEEE 26th International Symposium on Industrial Electronics (ISIE)*, 2017.

[53] M. Ahmed, L. Meegahapola, A. Vahidnia and M. Datta, "Stability and Control Aspects of Microgrid Architectures–A Comprehensive Review", *IEEE Access*, vol. 8, pp. 144730-144766, 2020.

[54] Y. Mohamed and E. El-Saadany, "Adaptive Decentralized Droop Controller to Preserve Power Sharing Stability of Paralleled Inverters in Distributed Generation Microgrids", *IEEE Transactions on Power Electronics*, vol. 23, no. 6, pp. 2806-2816, 2008.

[55] A. Subburaj, A. Arra and S. Bayne, "Stability Analysis of A.C. and D.C. Microgrids Using OPAL-Real Time Digital Simulator", *2017 Ninth Annual IEEE Green Technologies Conference (GreenTech)*, 2017.

[56] M. Prodanovic and T. Green, "Control and filter design of three-phase inverters for high power quality grid connection", *IEEE Transactions on Power Electronics*, vol. 18, no. 1, pp. 373-380, 2003.

[57] J. Enslin and P. Heskes, "Harmonic Interaction Between a Large Number of Distributed Power Inverters and the Distribution Network", *IEEE Transactions on Power Electronics*, vol. 19, no. 6, pp. 1586-1593, 2004.

[58] N.M. Tabatabaei, E. Kabalci and N. Bizon, "Microgrid architectures, control and protection methods", *Springer*, 2019.

[59] H. Bevrani, "Robust power system frequency control", 2014.

[60] T.T., Chan, "Transient analysis of integrated solar/diesel hybrid power system using MATLAB Simulink", 2008.

[61] H.L. Tsai, C.S. Tu and Y.J. Su., "Development of generalized photovoltaic model using MATLAB/SIMULINK", *Proceedings of the world congress on engineering and computer science*, vol. 2008, pp. 1-6, 2008.

[62] M. Petkov, D. Markova and S. Platikanov, "Modelling of Electrical Characteristics of Photovoltaic Power Supply Sources", *Contemporary Materials*, vol. 2, no. 2, pp. 171-177, 2011.

[63] Q. Zhao and F. C. Lee, "High-efficiency, high step-up DC-DC converters", *Power Electronics, IEEE Transactions on*, vol. 18, pp. 65-73, 2003.

[64] N. Mahamad, C. M. Hadzer and S. Masri, "Application of LC filter in harmonics reduction", *Proceedings of National Power and Energy Conference*, pp. 268–271, 2004.

Appendix A.

N_s	Number of PV modules connected in series	72
P_{pv}	Power generated by the PV system	0.6 p.u.
P_{pmsgw}	Power generated by the PMSG-based WECS	0.2 p.u.
P_a	Power generated by the microalternator	0.6 p.u.
P_l	Active power consumed by local load	0.8 p.u.
Q_l	Reactive power consumed by local load	0.2 p.u.
L_{dcpv}	DC/DC boost converter inductance of PV system	0.2 p.u.
R_{fpv}	Filter resistance of PV system	0.05 p.u.
L_{fpv}	Filter inductance of PV system	0.2 p.u.
C_{cpv}	Filter capacitance of PV system	0.2 p.u.
R_{drpv}	Filter damping resistance of PV system	0.02 p.u.
R_{copv}	Coupling line resistance of PV system	0.05 p.u.
L_{copv}	Coupling line inductance of PV system	0.2 p.u.
m_{pv}	Modulation index of inverter of PV system	1.02
H_{rw}	Inertial constant of rotor of PMSG	0.3
H_{tw}	Inertial constant of wind turbine	2
x_{dw}	d-axis synchronous reactance of PMSG	1 p.u.
x_{qw}	q-axis synchronous reactance of PMSG	0.7 p.u.
R_{fw}	Filter resistance of WECS	0.1 p.u.
L_{fw}	Filter inductance of WECS	0.2 p.u.
C_{cw}	Filter capacitance of WECS	0.2 p.u.
R_{drw}	Filter damping resistance of WECS	0.1 p.u.
R_{cow}	Coupling line resistance of WECS	0.1 p.u.
L_{cow}	Coupling line inductance of WECS	0.2 p.u.
m_{invw}	Modulation index of inverter of WECS	1.02
K_s	Stiffness constant of a two mass drive-train used in WECS	0.2
x_{da}	d-axis synchronous reactance of microalternator	1.3 p.u.

$x_{da}{}'$	d-axis transient reactance of microalternator	0.3 p.u.
x_{qa}	q-axis synchronous reactance of microalternator	0.47 p.u.
$T_{do}{}'$	Open-circuit field constant of microalternator	5
R_{ta}	Line resistance between microalternator and microgrid	0.1 p.u.
x_{ta}	Line reactance between microalternator and microgrid	0.2 p.u.
R_{stat}	Resistance of STATCOM	0.02 p.u.
L_{stat}	Inductance of STATCOM	0.2 p.u.
m_{stat}	Modulation index of STATCOM	1.02
R_g	Line resistance between microgrid and main grid	0.15 p.u.
x_g	Line reactance between microgrid and main grid	0.26522 p.u.